

# CPM-Based Radar Waveforms for Efficiently Bandlimiting a Transmitted Spectrum

*Matthew R. Cook*

Submitted to the graduate degree program in  
Electrical Engineering and Computer Science  
and the Graduate Faculty of the  
University of Kansas School of Engineering  
in partial fulfillment of the requirements  
for the degree of Master of Science

## Thesis Committee:

---

Dr. Shannon Blunt: Chairperson

---

Dr. Jim Stiles

---

Dr. Erik Perrins

---

Date Defended

The Thesis Committee for Matthew R. Cook certifies  
That this is the approved version of the following thesis:

**CPM-Based Radar Waveforms for Efficiently Bandlimiting a  
Transmitted Spectrum**

Committee:

---

Shannon Blunt

---

Jim Stiles

---

Erik Perrins

---

Date Approved

# Acknowledgments

First off, I would like to thank my advisor Dr. Blunt for his inspiration and faith in me to pursue an advanced degree. Not only has he encouraged me to expand my dreams and goals, he has provided the support and resources to do so. He emboldened me as an undergraduate student to reach my full potential and to continue my education. We have co-authored a conference paper together and are currently working on a subsequent journal article. Dr. Blunt has also encouraged my involvement in the radar community by funding my travels to the IEEE Radar Conference in 2009 where I was a presenter, and upcoming in 2010. I would like to thank Dr. Perrins for his considerable contribution to my knowledge and understanding of CPM. Dr. Perrins gave me my first research experience in the technical exploration of a CPM transmitter. He has been a dedicated instructor to me in and out of the classroom. I would also like to thank Dr. Stiles significant involvement in my education. I have had many classes with Dr. Stiles, and he is an instructor dedicated to purvey information in a complete and unambiguous nature. Dr. Stiles has also been an excellent role model as a professor as I have worked with him this year as his teaching assistant. I wish to thank my fellow students in the Radar and Remote Sensing Lab (Cenk, Geoff, Justin, Paul, and Tom) for their insight, corroboration, and friendship. Finally, with greatest importance, I would like to thank my wife Angela. Her unwavering faith in me has been a tremendous source of inspiration and motivation. She has been my pillar of strength through hard times and my biggest fan in my victories. Her devotion and support to the realization of my dreams has been an integral part of my success.

# Abstract

In this thesis it shall be demonstrated how a polyphase-coded radar waveform can be implemented using a continuous phase modulation (CPM) framework so as to achieve spectral containment while maintaining a constant envelope to maximize energy-on-target. Current implementations of waveforms such as derivative phase shift keying (DPSK) and minimum shift keying (MSK) are subject to spurious spectral components referred to as “spectral regrowth”. To design a waveform that removes these unwanted frequency components, the solution must not disturb the characteristics of the waveform to a point where it is no longer desirable to be used in the radar scenario, namely the power efficiency, range resolution, and target detectability. Power efficiency can be achieved by limiting choices to waveforms of constant modulus, or amplitude. The choice of a continuous phase waveform introduces a decrease in dynamic range. However, signal processing techniques will be presented as a means to increase the sensitivity. A version of the Least-Squares mismatch filtering will be implemented in a fashion that accommodates the continuous nature of the CPM structure. The DPSK and MSK techniques are applicable only to binary-coded waveforms. The CPM implementation will be formulated in a manner that gives it the added advantage of being applicable to polyphase-coded waveforms as well. The ability to utilize polyphase codes greatly increases the number of codes available, which is a direct benefit due to more diverse codes and longer code lengths. This trait can be exploited to use new longer polyphase codes increasing the pulse compression gain, hence target detectability. Results indicate that spectral spreading can be greatly decreased with the CPM implementation. The limiting factor on complete spectral containment for the CPM framework is the rise/fall-time as the waveform transitions on and off respectively. It will be shown that some tapering of the amplitude during these transition periods can be very beneficial in limiting spectral regrowth.

# Contents

Acceptance Page	i
Acknowledgments	ii
Abstract	iii
<b>1 Introduction</b>	<b>1</b>
<b>2 Background</b>	<b>5</b>
2.1 Radar Pulse Compression . . . . .	5
2.2 Ideal Radar Waveform . . . . .	7
2.3 Derivative Phase Shift Keying . . . . .	15
2.4 Minimum Shift Keying . . . . .	20
2.5 General CPM Model . . . . .	22
<b>3 Spectrally Efficient Implementation</b>	<b>30</b>
3.1 Radar CPM Model . . . . .	31
3.2 Rise-/Fall-Time Considerations . . . . .	37
<b>4 Receive Filter Implementation</b>	<b>45</b>
4.1 Matched Filter . . . . .	46
4.2 Mismatched Filter . . . . .	47
<b>5 Waveform/Filter Evaluation</b>	<b>56</b>
5.1 Receive Matched Filter Results . . . . .	57
5.1.1 Barker Waveforms . . . . .	57
5.1.2 Polyphase Barker Waveforms . . . . .	59

5.1.3	Minimum Peak Sidelobe Waveforms . . . . .	61
5.1.4	P-code Waveforms . . . . .	63
5.1.5	Nunn-Kretschmer Waveforms . . . . .	64
5.2	Receive Mismatch Filter Results . . . . .	66
5.2.1	Barker Waveforms . . . . .	66
5.2.2	Polyphase Barker Waveforms . . . . .	68
5.2.3	Minimum Peak Sidelobe Waveforms . . . . .	69
5.2.4	P-code Waveforms . . . . .	71
5.2.5	Nunn-Kretschmer Waveforms . . . . .	73
5.3	Spectral Analysis . . . . .	74
5.4	Experimental Results . . . . .	78
<b>6</b>	<b>Conclusion</b>	<b>80</b>
	<b>References</b>	<b>83</b>

# List of Figures

2.1	Ideal Signal for Length-5 Barker Sequence . . . . .	8
2.2	Basic Phase Modulator . . . . .	9
2.3	Autocorrelation for length-13 Barker code . . . . .	11
2.4	Sampled Waveform Sliding Through Comb Filter . . . . .	11
2.5	PSD for length-13 Barker code . . . . .	12
2.6	Autocorrelation for length-13 Polyphase Barker code . . . . .	14
2.7	PSD for length-13 Polyphase Barker code . . . . .	15
2.8	Phase Contrast Between Ideal Signal and DPSK Signal . . . . .	17
2.9	Receiver Matched Filter Output for Length-64 MPS code of DPSK vs. Ideal Waveforms . . . . .	18
2.10	PSD for length-64 MPS code of DPSK vs. Ideal . . . . .	19
2.11	Phase Contrast Between Ideal Signal and MSK Signal . . . . .	21
2.12	Receiver Matched Filter for length-64 MPS code of MSK vs. Ideal	23
2.13	PSD for length-64 MPS code of MSK vs. Ideal . . . . .	24
2.14	General CPM Block Diagram . . . . .	25
2.15	Phase Contrast Between Ideal Signal and CPM Signal . . . . .	26
2.16	Receiver Matched Filter for length-64 MPS code of CPM vs. Ideal	28
2.17	PSD for length-64 MPS code of CPM vs. Ideal . . . . .	29
3.1	Radar CPM Block Diagram . . . . .	31
3.2	Phase Contrast Between Ideal Signal and CPM Signal with Differ- ential Symbols . . . . .	33
3.3	Receiver Matched Filter Outputs for Ideal, Communications CPM, and Differential CPM Waveforms . . . . .	34
3.4	PSD for Ideal, Communications CPM, and Radar CPM Waveforms	35

3.5	Unwrapped Phase for the General CPM and Differential CPM Waveforms . . . . .	36
3.6	Two Amplitude Windows to Reduce Spectral Leakage . . . . .	38
3.7	PSD of Ideal, “On/Off” CPM, and CPM Windowed Waveforms . . . . .	41
3.8	PSD of Ideal, DPSK, MSK, and CPM Tukey Windowed Waveforms . . . . .	43
4.1	Ideal and CPM Receiver Mismatch Filter Output for length-64 Nunn-Kretschmer code . . . . .	49
4.2	Eigen-Spectrum of $(\mathbf{A}_{\text{CPM}}^H \mathbf{A}_{\text{CPM}})$ Using length-64 Nunn-Kretschmer code with $K = 10$ . . . . .	51
4.3	CPM Receiver Mismatch Filter Output Using length-64 Nunn-Kretschmer code with $K = 10$ . . . . .	52
4.4	CPM Receiver Mismatch Filter Output Using length-64 Nunn-Kretschmer code with $K = 10$ . . . . .	53
4.5	CPM Receiver Mismatch Filter Output Using length-64 Nunn-Kretschmer code with $K = 10$ and Spoiled Resolution . . . . .	54
4.6	CPM Receiver Mismatch Filter Output Using length-64 Nunn-Kretschmer code with $K = 10$ and Spoiled Resolution . . . . .	55
5.1	Receiver Matched Filter Results for Family of Barker-Coded CPM Waveforms . . . . .	58
5.2	Receiver Matched Filter Results for Family of Polyphase Barker-Coded CPM Waveforms . . . . .	60
5.3	Receiver Matched Filter Results for Family of MPS-Coded CPM Waveforms . . . . .	62
5.4	Receiver Matched Filter Results for Family of P-Code CPM Waveforms . . . . .	63
5.5	Receiver Matched Filter Results for Family of Nunn-Kretschmer CPM Waveforms . . . . .	65
5.6	Receiver Mismatch Filter Results for Family of Barker-Coded CPM Waveforms . . . . .	67
5.7	Receiver Mismatch Filtering Results for Polyphase Barker-Coded CPM Waveforms . . . . .	68
5.8	Receiver Mismatch Filter Results for Family of MPS-Coded CPM Waveforms . . . . .	70

5.9	Receiver Mismatch Filter Results for Family of P-Code CPM Waveforms . . . . .	72
5.10	Receiver Mismatch Filter Results for Family of Nunn-Kretschmer CPM Waveforms . . . . .	73
5.11	PSD Results for the Best PSL Performer of MPS, Polyphase Barker, P-Code, and Nunn-Kretschmer Codes . . . . .	75
5.12	PSD Results for the Best PSL Performer of MPS, Polyphase Barker, P-Code, and Nunn-Kretschmer Codes with Rectangular Chip Shaping Filter . . . . .	76
5.13	PSD Results for the Best PSL Performer of MPS, Polyphase Barker, P-Code, and Nunn-Kretschmer Codes with Tukey Amplitude Window . . . . .	77
5.14	Spectrum Analyzer Results for CPM Waveform . . . . .	78
5.15	Spectrum Analyzer Results for CPM Waveform . . . . .	79

# List of Tables

2.1	Barker Codes . . . . .	10
2.2	Length-64 Minimum Peak Sidelobe (MPS) code . . . . .	16
3.1	Nunn-Kretschmer Polyphase Code in Radians . . . . .	40
5.1	Receiver Matched Filter Results From Select Barker-Coded CPM Waveforms . . . . .	59
5.2	Receiver Matched Filter Results From Select Polyphase Barker-Coded CPM Waveforms . . . . .	61
5.3	Receiver Matched Filter Results From Select MPS-Coded CPM Waveforms . . . . .	61
5.4	Receiver Matched Filter Results From Select P-Code CPM Waveforms . . . . .	64
5.5	Results From the Family of Nunn-Kretschmer CPM Waveforms . . . . .	64
5.6	Mismatch Filter Results From Select Barker-Coded CPM Waveforms . . . . .	66
5.7	Mismatch Filter Results For Polyphase Barker-Coded CPM Waveforms . . . . .	69
5.8	Mismatch Filter Results From Select MPS-Coded CPM Waveforms . . . . .	71
5.9	Receiver Mismatch Filter Results From Select P-Code CPM Waveforms . . . . .	72
5.10	Results From the Family of Nunn-Kretschmer CPM Waveforms . . . . .	74

# Chapter 1

## Introduction

The need for efficient use of the electromagnetic radio-frequency spectrum has never had as great of an importance as it commands today. Advancements in technology are still accelerating and new devices and equipment are all requiring use of the spectrum as wireless technologies become prevalent. In the radar community, commonly used waveforms are chosen for their efficient use by high power amplifiers in radar pulse compression, are notorious for being spectrally inefficient, generating spurious frequencies over large frequency bands. The goal of this research is to find a new method of generating radar waveforms that preserves the needed characteristics of power efficiency, high range resolution and target detectability, while removing the extraneous bandwidth. Some degradation in dynamic range is expected from a decrease in bandwidth, but signal processing techniques can be employed to counter some of the negative byproducts.

Many approaches have been explored in order to create a radar waveform that can enhance the target features that can be extracted from the radar echo. For the reader who is not familiar with basic radar concepts, refer to [1]. One must consider which features are more important in designing the waveform. Certain

engineering trade-offs present themselves such as waveform bandwidth and range resolution, or pulse width and frequency resolution. One thing is certain, for the transmitted waveform to be considered practical and useful, a fidelity measure of the extracted features must be met at a level described in the design criteria specified for the situation at hand. Further, the ideal characteristics used to generate and simulate said waveforms must be physically realizable once implemented on real world systems. This limitation should not be overlooked.

In the United States, the governing body that allocates and restricts use of the electromagnetic spectrum is the U.S. Department of Commerce's National Telecommunications and Information Administration (NTIA). The Radar Spectrum Engineering Criteria, or RSEC, states in Section 5.5.2, part 3.1 in the 2008 version that FM-pulse radars, including spread spectrum and coded pulse radars, have a -40 dB emission bandwidth limit of

$$B(-40 \text{ dB}) = \frac{7.6}{\sqrt{t_r t}} \quad \text{or} \quad \frac{64}{t}, \quad (1.1)$$

whichever is less, where  $t$  is the emitted pulse duration in microseconds at the 50% amplitude (voltage) points. This is the interval between the 50% amplitude points of one chip (sub-pulse) for coded pulses. The 100% amplitude is the nominal flat top level of the pulse. The emitted pulse rise time,  $t_r$ , is measured in microseconds and defined as the time from the 10% to the 90% amplitude points on the leading edge. This is the defined rise-time of a sub-pulse for coded pulses. If the sub-pulse rise-time is not discernible, it is assumed that the rise-time is 40% of the time to switch from one phase or sub-pulse to the next.

The task of confining the spectral spreading to a bandwidth prescribed by a pre-defined spectral mask such as in the RSEC has long been approached by a cost-

effective method of pre-distortion. Out-of-band suppression of -100 dB has been a challenge that calls for tight and stable tolerances in the pre-distortion method. In digital communications, modulation schemes such as Gaussian minimum shift keying (GMSK) or quadrature phase shift keying (QPSK) must be designed to fit certain mutual non-interference requirements defined by a spectral mask. The out-of-band suppression requirements have yet to be established for radar, but the relationship in (1.1) provides a guideline. A goal of -100 dB suppression shall be considered more than sufficient for the work presented here. Thus the purpose of this work is to develop a new method of generating radar waveforms, utilizing the techniques that have been proven to be spectrally efficient in the communications community. While a direct application is not fitting to the radar waveform, a generalization can be made. Then a radar model will be developed keeping the spectrally efficient traits, whilst incorporating attributes necessary to create a “good” radar waveform.

In this thesis, Chapter 2 introduces a background on radar codes and waveforms presented to give the reader the necessary understanding of what is currently considered for implementation in today’s radar systems. Then a comparison will be made with a modulation scheme that has been used extensively in the communication arena, continuous phase modulation (CPM), as a means to achieve power and spectral efficiency. In Chapter 3 a new CPM framework will be introduced to form a model that best fits the current radar implementations, while preserving the gains achieved in spectral containment. Chapter 4 implements a method of receive filtering that is presented to reduce negative byproducts of the CPM framework such as increased range sidelobes and range resolution. Finally, the results of several radar codes will be analyzed in Chapter 5. Characteristics

examined are peak sidelobe levels, integrated sidelobe levels and mainlobe widths of the radar range profile, as well as the power spectral densities of the modulated waveforms.

# Chapter 2

## Background

### 2.1 Radar Pulse Compression

In the design of a practical and useful radar waveform, three categories are desired to have maximum performance. These factors are target detection, dynamic range (range and Doppler) and resolution (range and Doppler). In the pursuit of maximizing the overall performance of the waveform, a fundamental trade-off of radar waveform design is encountered. Target detection is dependent upon the signal-to-noise ratio (SNR) of the received reflection. This means that the total energy delivered to the target, or energy-on-target, must be relatively large. However, good performance in accuracy and resolution require not only sufficient energy-on-target, but a large bandwidth as well. This translates to a radar pulse of relatively short duration with a large peak power. These properties are not desirable, because large peak powers are not always available and Doppler resolution is inversely proportional to pulse length [2].

One method to increase the energy delivered to a potential target while maintaining accuracy and resolution available from a short pulse is to use radar pulse

compression. In pulse compression the pulse is a modulated series of chips transmitted together sequentially. This is the “discrete” version of radar waveforms. When the receive filter is matched to the sub-pulses in the waveform the energy from all of the sub-pulses is combined into one large return with the extent of only a single sub-pulse. Pulse compression waveforms come in many different varieties, but these can be broken down into two general classes. The first class is linear frequency modulation (LFM) pulse compression, commonly referred to as a chirp. These are the more classically “continuous” radar waveforms. This basic concept of LFM was described in a patent filed in 1945 (issued in 1953) by R. H. Dicke [1]. The second class is a collection of phase-coded pulses. In the past, binary phase has been the most common code types, but polyphase codes are becoming more attractive as new signal processing techniques are being developed to exploit the added diversity. The reason for added interest in polyphase codes is due to the increased number of available codes and the greater lengths that are possible in the codes.

Other pulse compression schemes include Costas codes, nonlinear FM pulse compression, nonlinear binary phase-coded sequences, complementary codes (Golay codes), Welton codes and Huffman codes to name a few. A code is generally chosen to fit the aspects of the radar scenario being addressed, while maximizing the reduction of time sidelobes. Time sidelobes are a byproduct of pulse compression that are not encountered when using a single short pulse. These sidelobes can be troublesome by being mistook for targets or masking smaller targets in close proximity to larger targets. The amplitude and phasing of the uncompressed pulse determines the size and extent of the sidelobes. Therefore, choice of the radar waveform is crucial to successful pulse compression.

## 2.2 Ideal Radar Waveform

There are two sides to consider in radar waveform design that depend greatly on the application. One must decide if the waveform will be based on continuous or discrete characteristics. However, it can never be overlooked that this waveform will be transmitted from a real antenna. So the waveform is always continuous and subject to the associated realistic electromagnetic limitations. That being said, expanding design criteria to discrete calculations offers numerous benefits that can be exploited. Many radar systems employ naturally occurring continuous waveforms. Linear frequency modulation (LFM) waveforms offer good range and frequency resolution with modest spectral spreading. But the cost is that the peak sidelobe level (PSL) and integrated sidelobe level (ISL) may not meet the requirements of many radar applications. If restrictions on the bandwidth of the waveform are lessened, a discrete-like waveform can be modulated that can have a very small PSL given a properly chosen receive filter. While the benefits cannot be completely achieved in practice, a waveform can be realized that characterizes the general concept of the discrete waveform design.

The classical definition of an ideal discrete radar waveform is one in which the chip, or phase, value is held constant throughout the duration of the chip interval. Discrete phase codes are used in this manner to implement a “discrete” waveform in the continuous-time domain. Upon transition to the next phase value the baseband waveform’s phase transitions instantaneously. In theory, this ideal waveform can have excellent autocorrelation properties for a properly chosen phase code, yet it is physically unrealizable. A mathematical formulation of this

“ideal” waveform is

$$s_{\text{IDEAL}}(t) = \sum_{n=0}^{N-1} e^{jx(n)} [u(t - n\tau) - u(t - (n + 1)\tau)], \quad (2.1)$$

where  $\tau$  is the chip interval and  $u(t)$  is the unit step function [3]. The waveform  $s_{\text{IDEAL}}(t)$  will be denoted as the Ideal waveform. The phase values are contained in the phase code  $x(n)$  which has  $N$  phase values, where  $x(n) \in [0, 2\pi]$ . For example, using a length-5 Barker sequence as the phase code, the “ideal” waveform described in (2.1) is shown in Figure 2.1, where the phases are shown above each chip.

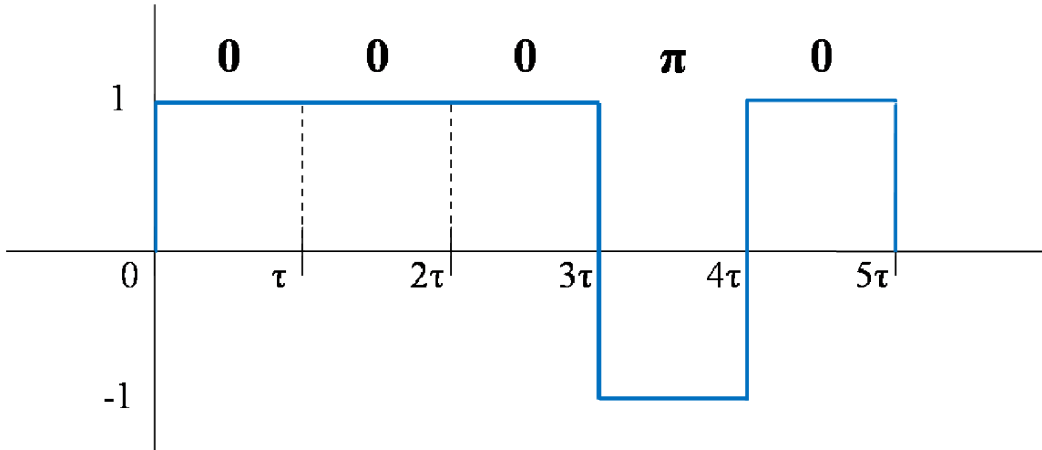


**Figure 2.1.** Ideal Signal for Length-5 Barker Sequence

A distinction must be made to clarify the difference when referring to a radar code and a radar waveform. A radar code is a sequence of discrete values, in most cases phase values, ordered in such a way as to create an optimality in some chosen sense, such as PSL. Conversely, a radar waveform is the physical modulation on an electromagnetic wave embedded with the information of the radar code, by

some chosen means of implementation, such as phase-shift keying modulation.

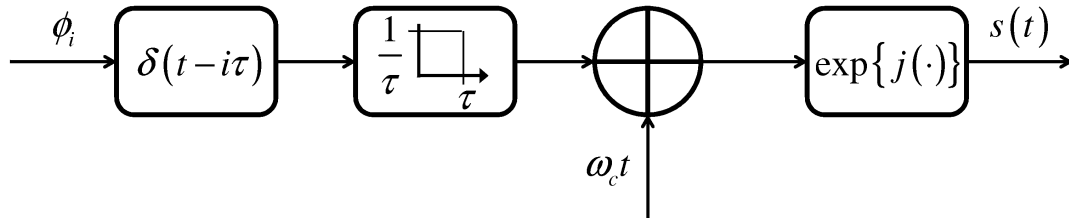


**Figure 2.2.** Basic Phase Modulator

A block diagram for a basic ideal modulator is shown in Figure 2.2. The first block represents an impulse train with the number of impulses equaling the number of chips and spaced by the chip interval. The impulse train is then filtered with an ideal rectangular filter. This result becomes the phase of the waveform (assuming the initial phase of the system is 0 without loss of generality). The carrier phase is then added in and the sum becomes the argument of the complex exponential. This output is the ideal discrete waveform. So it becomes clear that for  $s(t)$  to be a “good” radar waveform, the code  $\phi_i$  must be chosen carefully.

The topic of radar coding has been researched in depth. Codes such as Barker, Polyphase Barker, Minimum Peak Sidelobe, and Frank codes have been considered [4–6]. Further, new methods of code design have been developed recently [7, 8]. These codes as well as many others provide good autocorrelation properties, but have been designed on the notion of an idealistic waveform (*i.e.* instantaneous transitions). Such a waveform cannot be physically transmitted, but the properties of these codes are still retained to some degree even with a realizable waveform. Deviation from the “ideal” waveform could introduce degradation on receive, specifically increased range sidelobes and loss of dynamic range.

However, these problems may be addressed with the application of appropriate signal processing in the receiver.

Barker codes are perhaps the most recognized family of radar codes. First developed by Barker in 1953, this collection of codes consist of  $M$  binary phase values and possesses the property of having a PSL of  $\frac{1}{M}$ . The limiting factor of these codes is that it has been shown that no Barker codes exist for odd  $M > 13$  and all  $13 < M < 1898884$ . No Barker codes exist for  $M > 13$ , though no mathematical proof yet exists [4]. The known Barker codes are listed in Table 2.1. The problem with having so few phase values in a code is that sufficient energy on

**Table 2.1.** Barker Codes

M	Code
2	11 or 10
3	110
4	1110 or 1101
5	11101
7	1110010
11	11100010010
13	1111100110101

the target cannot be provided to achieve the required signal to noise ratio (SNR) without affecting the radar's range resolution. A plot of the autocorrelation for a length-13 Barker code is shown in Figure 2.3. Note the uniform structure of the results. Each sidelobe has a normalized value of  $\frac{1}{13}$ , or -22.3 dB, with 0, or  $-\infty$  dB in between. The square shape of the lobes is due to the structure of the filter used. A comb-structure was used with matched filter values spaced one chip interval apart. This is illustrated in Figure 2.4 by showing an arbitrary waveform with 3 samples per chip sliding through a comb structured filter. Filter coefficients are spaced at coordinated 3 sample intervals with zero filling in between coefficients.

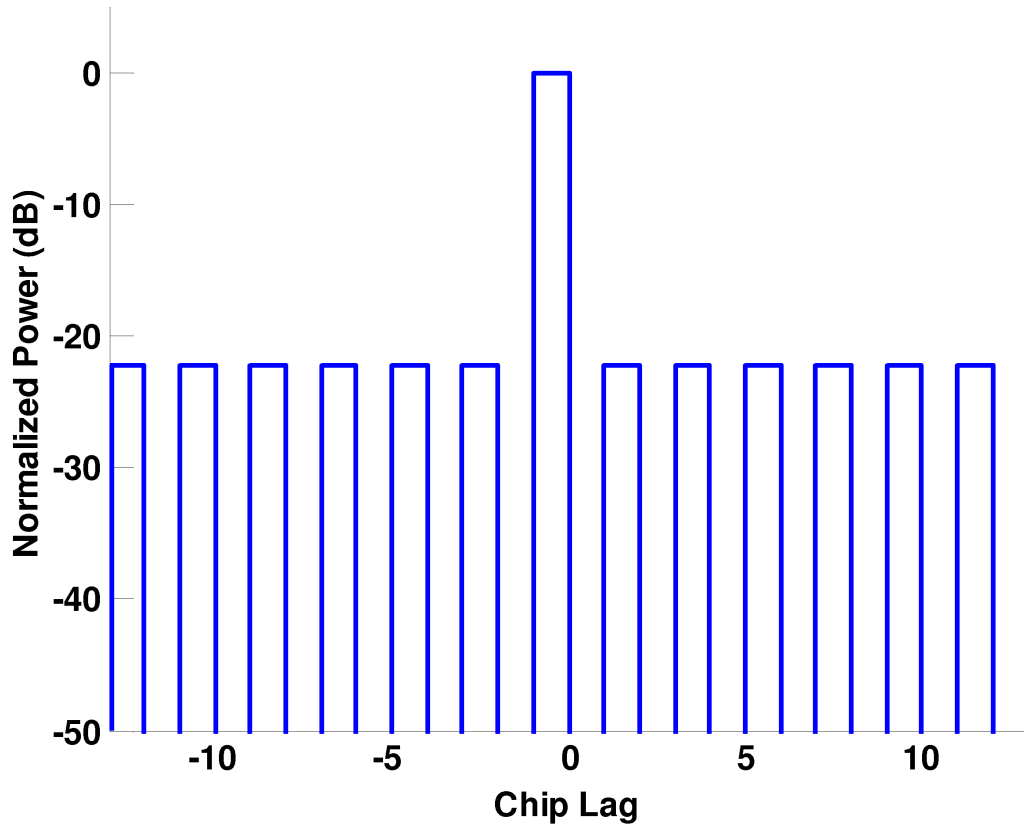


Figure 2.3. Autocorrelation for length-13 Barker code

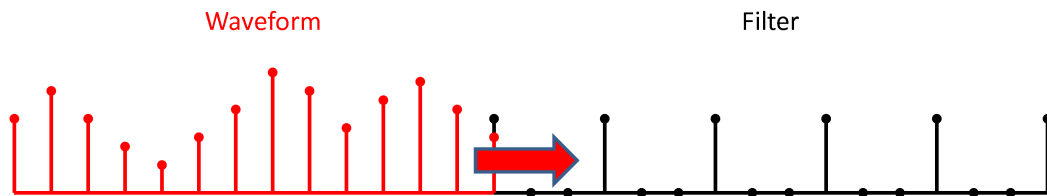


Figure 2.4. Sampled Waveform Sliding Through Comb Filter

There is a downside to this code, though. To get such sidelobe suppression the chip shapes are those of the ideal code in (2.1). Taking the Fourier transform of this sampled waveform and examining the power spectral density (PSD) shows that large spectral sidelobes are present. The PSD of the length-13 Barker coded ideal waveform is shown in Figure 2.5. There are nulls at harmonic multiples

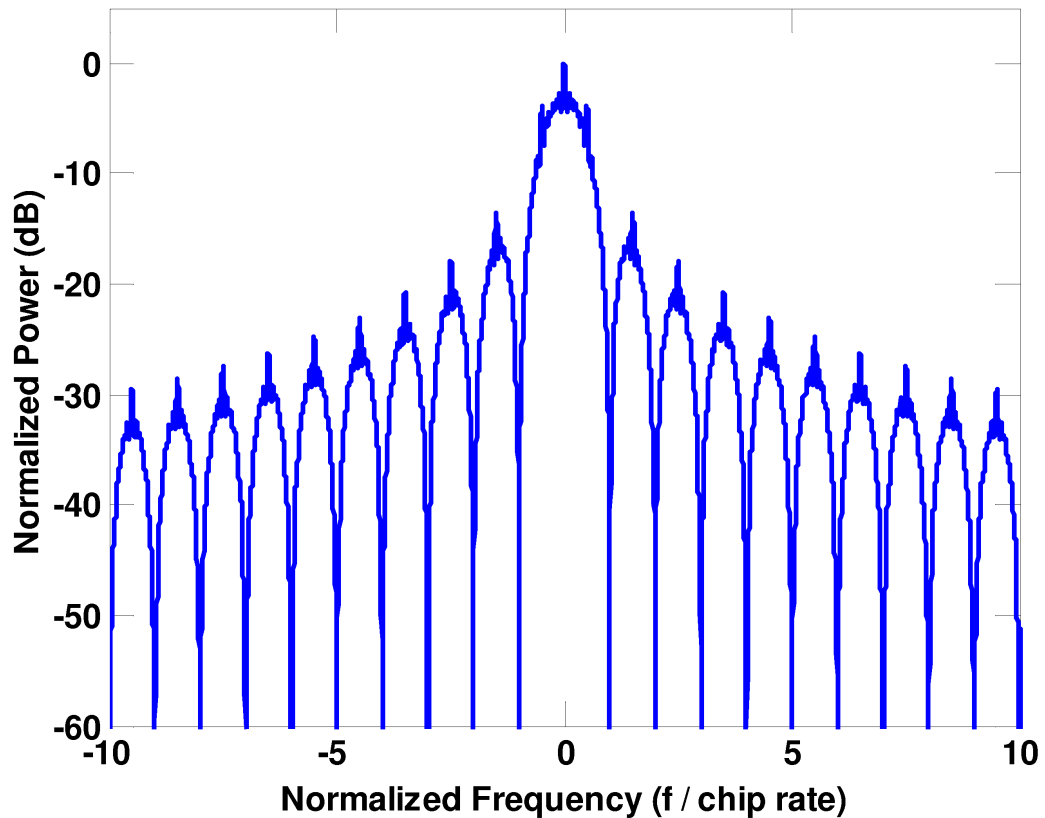
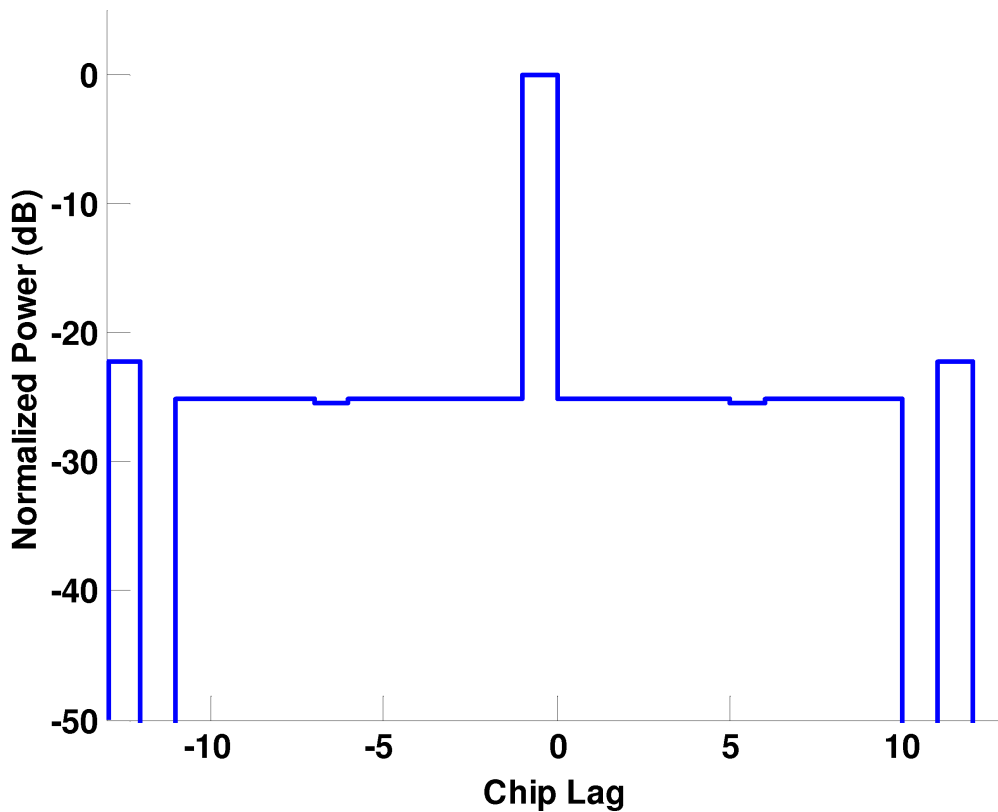


Figure 2.5. PSD for length-13 Barker code

of the chip frequency. Halfway between the harmonics of the chip frequency are spikes centered in the spectral sidelobes. There is also a spike at the center of the mainlobe. These spikes are due to the phase shifts in the waveform consisting of only  $\pi$  radians. The peak of the first spectral sidelobe is at -13.5 dB at a frequency

of 1.5 times the chip rate. At 9.5 times the chip rate the spectral sidelobes are peaking at -29.5 dB.

Polyphase Barker codes were first considered by Frank [5]. He proposed that by letting the code take on more phase values than just 0 and  $\pi$ , the additional degrees of freedom would allow codes to be found that are longer than the limited Barker codes. These new codes could have any phase value in the  $2\pi$  space and the PSL must be less than or equal to  $\frac{1}{M}$ , where  $M$  is the number of code elements. Polyphase Barker codes have been found up to length 77 [9], which is a significant improvement on the longest known biphasic Barker code of length 13. To illustrate the advantage of the extra degrees of freedom contained in a polyphase Barker code, the autocorrelation for the waveform of a length-13 code is shown in Figure 2.6. It can be seen in the figure that the outermost sidelobe has a value of -22.3 dB at  $\pm 12\tau$ . This is expected, because the outermost sidelobe of any polyphase or binary code will have a value of  $\frac{1}{M}$  for an  $M$ -length code normalized to a peak value of 1 [4]. If this sidelobe is omitted, the PSL for this polyphase Barker waveform is 0.72. If the autocorrelation is normalized by  $\frac{1}{M}$ , this is a PSL of approximately -25.12 dB. This is observed in Figure 2.6. The spectral properties of the polyphase Barker waveform should be similar to those of the biphasic Barker waveform. Figure 2.7 shows that the spikes centered on the spectral lobes seen in Figure 2.5 are now gone. This is congruent with the idea that they occur from  $\pi$  phase shifts, because the phase shifts are now less than  $\pi$ . The first spectral peak is at approximately -14.5 dB from the mainlobe peak and the peak at 9.5 times the chip frequency is approximately -30.5 dB from the mainlobe peak. Compared to the biphasic length-13 Barker code, the spectral envelope of the polyphase length-13 Barker is about 1 dB smaller. This is mainly due to the absence of the spikes



**Figure 2.6.** Autocorrelation for length-13 Polyphase Barker code

centered between the harmonic multiples of the chip frequency.

If the idea of polyphase Barker codes is expanded to a less restrictive PSL constraint, even longer codes can be found. The peak sidelobe must be a sufficiently small value for the code to be considered good, but not necessarily smaller than the  $\frac{1}{M}$  level associated with the Barker criterion. Binary codes such as these are often referred to as minimum peak sidelobe (MPS) codes. In Table 2.2 a length-64 MPS code is listed [4]. This code will be used as a test example for comparing binary modulation techniques in Sections 2.3 – 2.5.

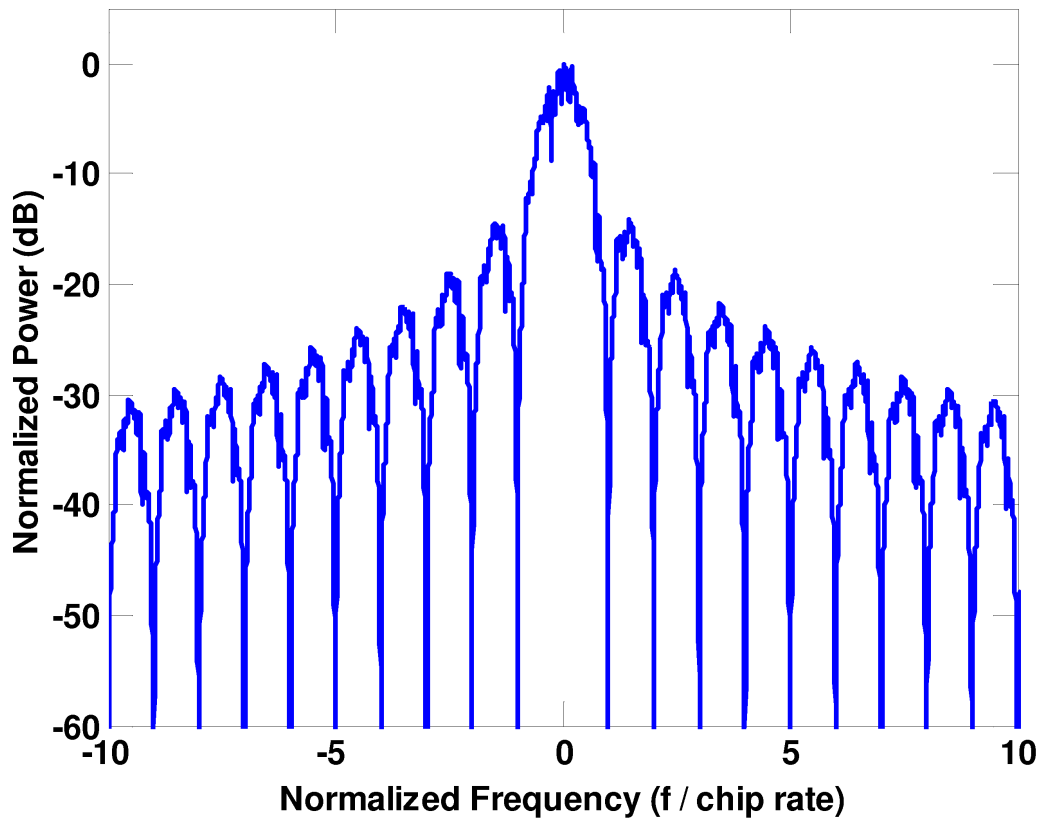


Figure 2.7. PSD for length-13 Polyphase Barker code

### 2.3 Derivative Phase Shift Keying

A common modulation scheme used in radar pulse compression is derivative phase shift keying (DPSK). DPSK is a binary modulation that offers better spectral containment by removing the unwanted phase jumps encountered in phase shift keying (PSK) which were discussed briefly in Section 2.2. A DPSK modulated waveform is a continuous waveform, but has a discontinuous first derivative that limits the amount of spectral containment it can offer. DPSK modulation

**Table 2.2.** Length-64 Minimum Peak Sidelobe (MPS) code

Chip	Phase	Chip	Phase	Chip	Phase	Chip	Phase
1	$\pi$	17	0	33	0	49	$\pi$
2	0	18	$\pi$	34	0	50	$\pi$
3	$\pi$	19	0	35	0	51	0
4	$\pi$	20	$\pi$	36	$\pi$	52	0
5	$\pi$	21	$\pi$	37	$\pi$	53	$\pi$
6	$\pi$	22	$\pi$	38	0	54	0
7	$\pi$	23	0	39	0	55	0
8	$\pi$	24	$\pi$	40	$\pi$	56	0
9	0	25	0	41	$\pi$	57	0
10	$\pi$	26	0	42	$\pi$	58	0
11	$\pi$	27	0	43	0	59	$\pi$
12	0	28	$\pi$	44	0	60	$\pi$
13	$\pi$	29	0	45	$\pi$	61	$\pi$
14	$\pi$	30	$\pi$	46	$\pi$	62	$\pi$
15	$\pi$	31	$\pi$	47	0	63	0
16	$\pi$	32	0	48	$\pi$	64	$\pi$

can be expressed mathematically as [3]

$$s_{\text{DPSK}} = s_{\text{IDEAL}} \left( t - \frac{\tau}{2} \right) \left| \cos \left( \frac{\pi t}{\tau} \right) \right| - j s_{\text{IDEAL}}(t) \left| \sin \left( \frac{\pi t}{\tau} \right) \right|. \quad (2.2)$$

For DPSK modulation the phase code must be binary (*i.e.*  $x(n) \in \{0, \pi\}$ ). Also, the starting phase of the waveform must be initialized with the first value of the phase code. To contrast the difference in phase transitions between the “ideal” modulation and the DPSK modulation, consider again the length-5 Barker sequence. Figure 2.8 depicts this contrast by showing how the DPSK waveform’s phase transitions  $\frac{\pi}{2}$  radians then back for two successive symbols that are the same. But when the two successive symbols are different the phase transitions  $\pi$  radians during the chip period  $\tau$ . The Ideal waveform has a constant phase for the first 3 chips. But for the fourth phase interval the Ideal waveform’s phase

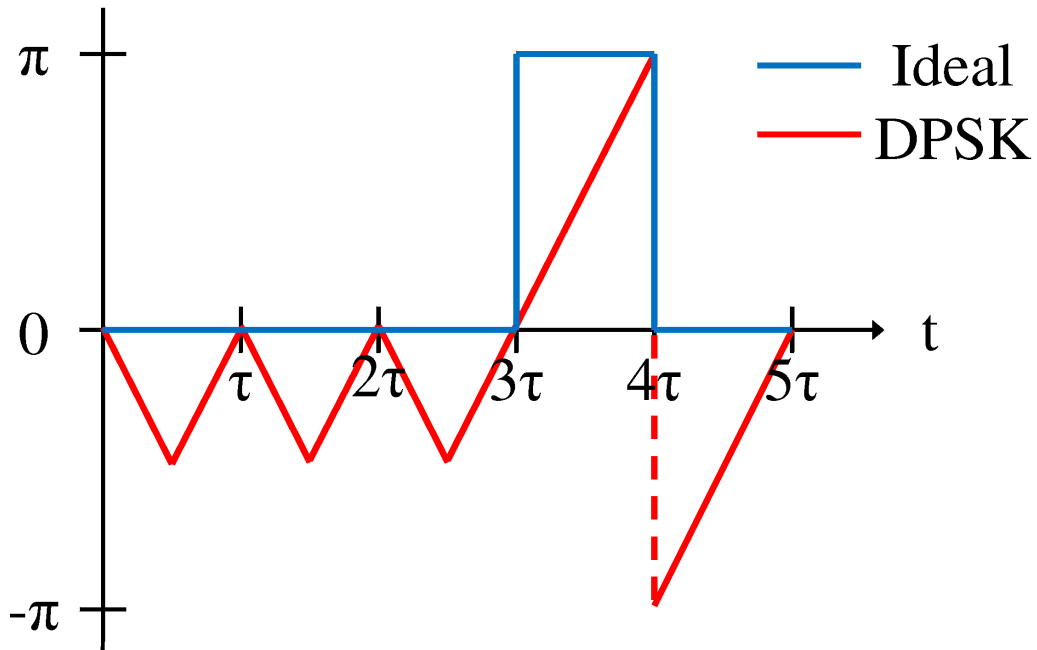


**Figure 2.8.** Phase Contrast Between Ideal Signal and DPSK Signal

instantaneously transitions to  $\pi$  then transitions back to 0 at the beginning of the fifth interval.

To demonstrate differences in receiver matched filter output and spectral content between the Ideal waveform and the DPSK waveform, the length-64 MPS code in Table 2.2 is considered. The first comparison is the receiver matched filter output plotted in Figure 2.9. The matched filter possesses one sample per chip taken from the phase code. This will result in the comb filter shape shown in Figure 2.4. It is evident that the correlation properties of the DPSK waveform hold close to the ideal waveform. There is a loss of approximately 2 dB in PSL for the DPSK waveform. Where the benefit of DPSK lies is in the decrease of spectral sidelobes. Because of the linear  $90^\circ$  phase transitions the bandwidth is

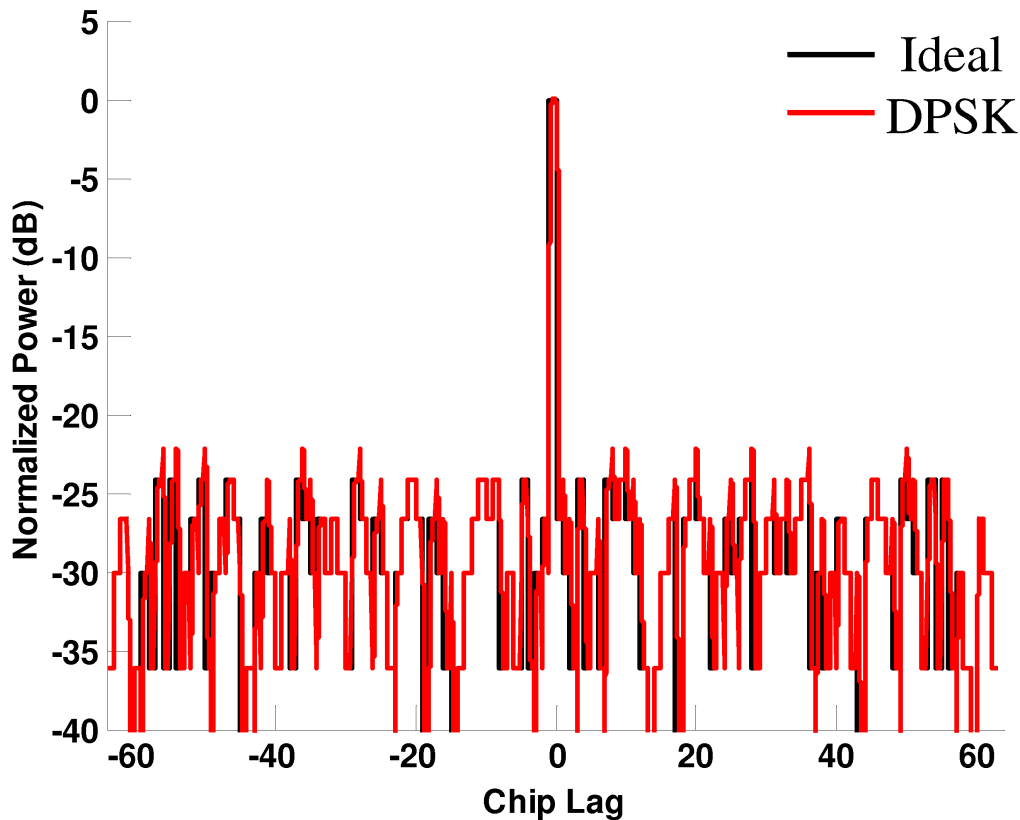


**Figure 2.9.** Receiver Matched Filter Output for Length-64 MPS code of DPSK vs. Ideal Waveforms

reduced ( The PSD is shown in Figure 2.10). Due to the finite length of the waveform, and the idealistic rise-/fall-time of the pulse, infinite spectral content is still observed. Also note that the spectrum is shifted for DPSK. While the reason for the shift is not clear at this time, similar results were previously seen in [10]. DPSK has comparable spectral content to the chip frequency. Beyond that the Ideal waveform's spectrum slowly rolls off while DPSK's spectrum drops off much faster. The first spectral sidelobe of DPSK is at -10 dB down from the peak. This occurs at the negative of the chip frequency (since this is a baseband waveform). The Ideal waveform's first spectral peak is about -13 dB down from the peak, a

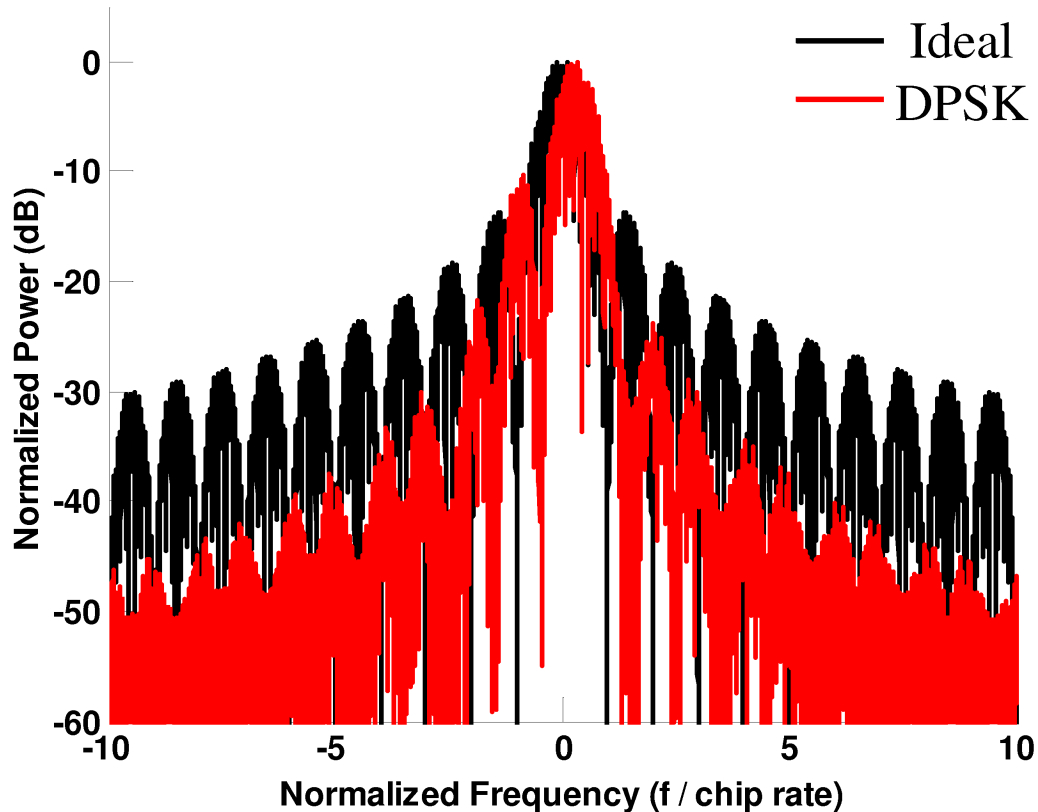


**Figure 2.10.** PSD for length-64 MPS code of DPSK vs. Ideal

decrease of 3 dB, but at 1.5 times the negative of the chip frequency. So comparatively, the envelope of both spectra is virtually the same in a bandwidth of 2 times the chip frequency centered at 0 for the baseband waveform. At 2 times the chip frequency the Ideal PSD is at about -18 dB, compared to the DPSK spectral power at -21 dB from the peak. Around 9.5 times the chip frequency the Ideal waveform's spectrum is at a level of about -30 dB from the peak. The DPSK waveform's spectrum is approximately -45 dB from the peak around 9 times the chip frequency. It is clear that DPSK has much better spectral containment, and the range sidelobes have incurred only a slight increase in PSL compared to the

Ideal case.

## 2.4 Minimum Shift Keying

A second modulation type used in radar pulse compression to suppress spectral sidelobes is minimum shift keying (MSK). MSK is also known as fast frequency shift keying (Fast FSK). MSK can be viewed as a special case of continuous phase modulation, but can also be cast as an offset quadrature scheme [11]. As a quadrature scheme, the binary data stream is divided into odd and even symbols defined over a double interval  $2T$  as

$$a_I(t) = \alpha_n, \quad (n-1)T < t \leq (n+1)T \quad \text{for even } n, \quad (2.3)$$

$$a_Q(t) = \alpha_n, \quad (n-1)T < t \leq (n+1)T \quad \text{for odd } n, \quad (2.4)$$

where

$$\alpha_n = e^{jx(n)}. \quad (2.5)$$

Using (2.3) and (2.4) the MSK signal is defined as

$$s_{\text{MSK}}(t) = (2E/T)^{1/2} [a_I(t) \cos(\pi t/2T) \cos \omega_0 t + a_Q(t) \sin(\pi t/2T) \sin \omega_0 t]. \quad (2.6)$$

For MSK the input symbols are defined in the sequence  $\alpha(n) = \alpha_n$ , which comes directly from the phase code  $x(n)$ . The MSK symbols differ from the two previous waveforms defined in (2.1) and (2.2) because the symbols come from an antipodal set,  $\alpha_n \in \{-1, 1\}$ , whereas the values for DPSK and the ideal modulation are taken directly from the radar code from the set  $x(n) \in \{0, 1\}$ . If  $\alpha_n = 1$ , the phase of the MSK signal advances  $+\frac{\pi}{2}$  radians. Conversely, if  $\alpha_n = -1$  the signal

delays by  $-\frac{\pi}{2}$  radians. For the same length-5 Barker code previously used in Sections 2.2 and 2.3, the phase transitions are shown in Figure 2.11 for the MSK implementation. Note that the phase of the MSK waveform has been wrapped to

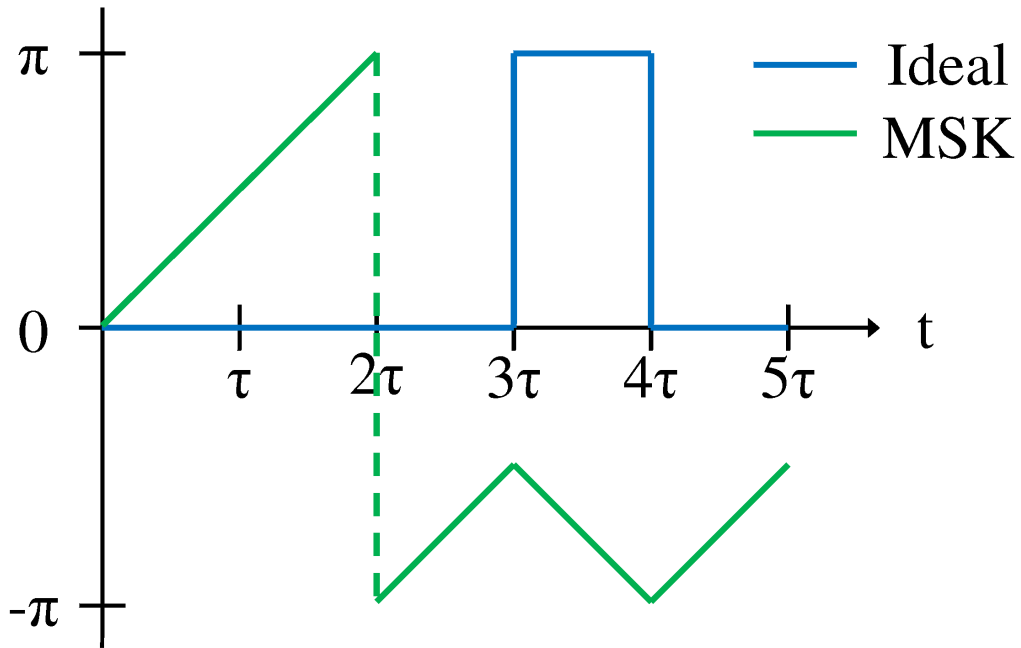


**Figure 2.11.** Phase Contrast Between Ideal Signal and MSK Signal

confine the phase in the plot between  $-\pi$  and  $\pi$ . It is evident that the phase of the MSK waveform is continuously moving, whilst the Ideal waveform's phase moves to  $\pi$  only during the 4<sup>th</sup> chip interval. The information contained in the phase of the Ideal waveform has been mapped into positive and negative frequency shifts. The MSK waveform exhibits a positive frequency shift corresponding to a phase of  $0$  in the Ideal waveform, and a negative frequency shift corresponding to a phase of  $\pi$  in the Ideal waveform.

To continue the comparison with the Ideal waveform, the length-64 MPS code

will be used again to simulate the receiver matched filter output and the PSD of the Ideal and MSK waveforms. The result of the filtered MSK waveform is shown in Figure 2.12. It should be noted that the matched filter for DPSK and the Ideal waveform was implemented based on one sample per chip of the Ideal waveform (*i.e.* the radar code). However, if the phase transitions are examined in Figure 2.11, and based upon the characteristic that MSK shifts  $\pm\frac{\pi}{2}$  radians every chip interval, it is evident that the matched filter structure for MSK waveform must be based on this waveform implementation. For the matched filter response shown in Figure 2.12, the matched filter for the MSK output was taken from the first sample of each chip interval, then up-sampled to the comb filter structure shown in Figure 2.4. Comparisons were made by taking samples from the beginning, middle and end of the chip interval for the matched filter, and it was found that taking samples from the beginning of the interval gives the best results. The matched filter for the ideal output was still taken directly from the phase values of the code. The MSK output shows a normalized PSL of approximately -17 dB, an increase of 7 dB from the output of the Ideal case.

Figure 2.13 shows the simulated PSD for the MSK waveform versus the Ideal waveform. Here the benefits of MSK are evident. The spectral sidelobes have been greatly reduced, but at the cost of increased range sidelobes. The peak of the first spectral sidelobe of the MSK waveform is at -23 dB. Compared to the first sidelobe of the Ideal waveform of -13.6 dB, this is a decrease of 9.4 dB.

## 2.5 General CPM Model

In aeronautical telemetry and Bluetooth applications, continuous phase modulation (CPM) is extensively used to maintain power and spectral efficiency. CPM

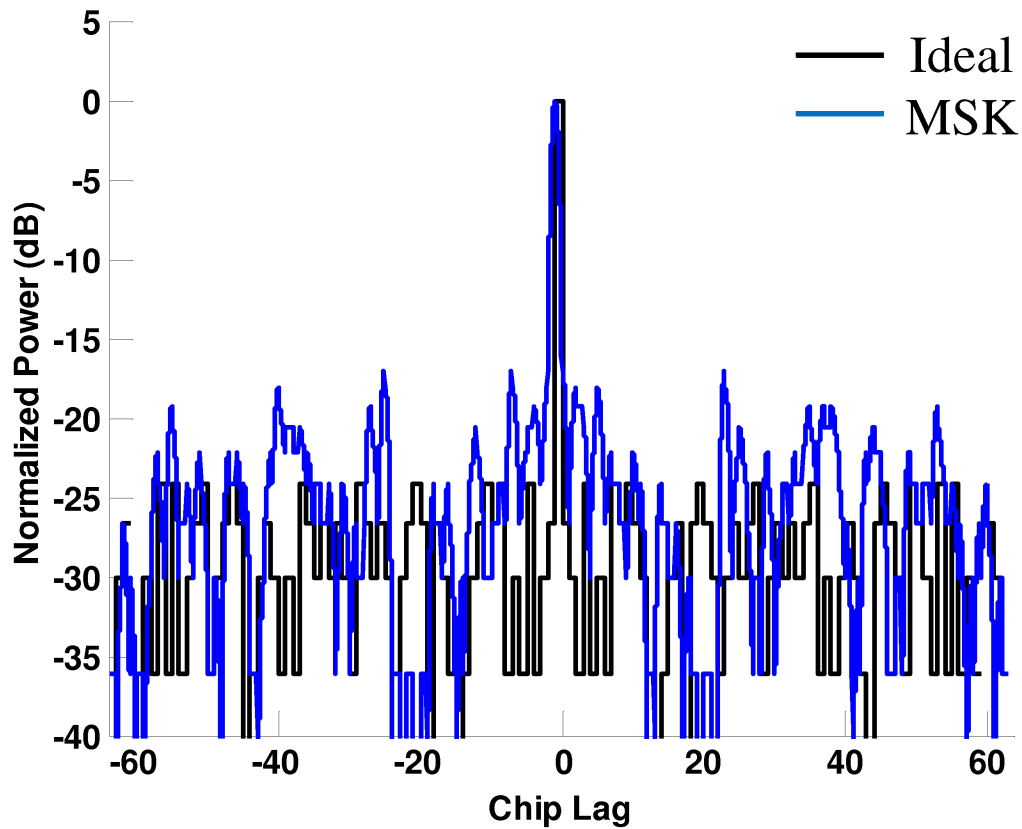


**Figure 2.12.** Receiver Matched Filter for length-64 MPS code of MSK vs. Ideal

is a twist on phase shift keying (PSK) that involves the use of memory and an integrator. For the PSK waveform, the phase of the signal is that of the “ideal” radar waveform described in Equation 2.1 and shown in Figure 2.1. The PSK waveform would require infinite bandwidth to make such instantaneous phase jumps, and is not physically realizable. To decrease the required bandwidth needed for the transmitted radar signal, while maintaining power efficiency, CPM is proposed as a means to modulate any arbitrary polyphase radar code.

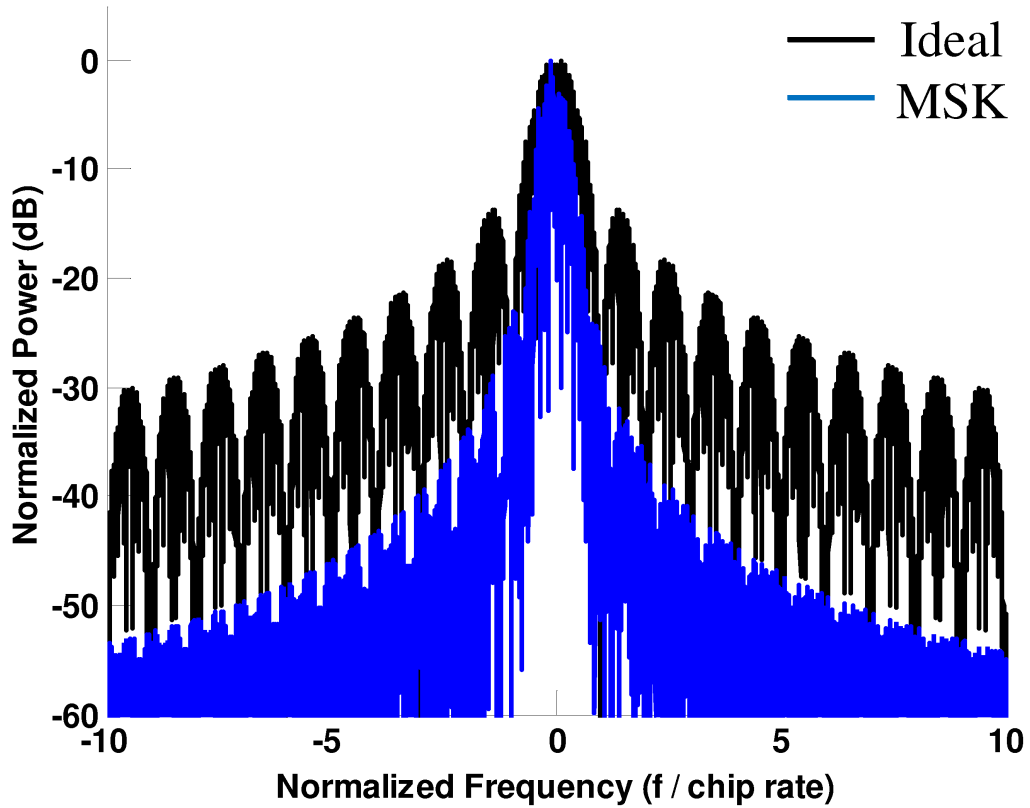


Figure 2.13. PSD for length-64 MPS code of MSK vs. Ideal

CPM signals can be represented by a single equation [11],

$$s(t) = (2E/T)^{1/2} \cos \left[ \omega_0 t + 2\pi \sum_{i=0}^n \alpha_i h_i q(t - iT) \right], \quad nT < t < (n+1)T. \quad (2.7)$$

As it is employed in communications,  $\{\alpha_i\}$  represents M-ary data symbols,  $h_i$  is the modulation index, and  $q(\cdot)$  is the phase response function. The use of a subscripted modulation index allows for multi- $h$  modulation, in which the modulation index can be changed from symbol to symbol. The omittance of subscript on the modulation index implies single- $h$  modulation where the value remains constant throughout the modulation. This CPM model allows for the implementation of a

real valued signal with a carrier frequency. However, the scope of this work will take the approach of dealing with complex baseband signals. Further, signals will be normalized to have unit energy per symbol, thus

$$E/T = 1. \quad (2.8)$$

A block diagram of a general CPM modulator is shown in Figure 2.14.

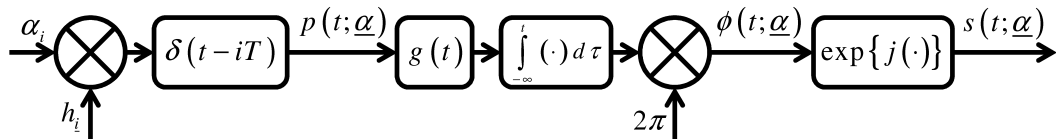


**Figure 2.14.** General CPM Block Diagram

One particular difference between MSK and the CPM used here, similar to shaped offset quadrature phase shift keying (SOQPSK) [12], is that ternary code elements<sup>1</sup> from the set  $\alpha_n \in \{-1, 0, 1\}$  are used. In Section 3.1 the CPM model will be relaxed to take on arbitrary symbol values. This difference can be shown in the phase trajectory of the CPM waveform, when using a linear phase response function. Using the length-5 Barker code, the phase of the CPM waveform versus the Ideal waveform's phase is shown in Figure 2.15. In contrast to the MSK phase trajectory shown in Figure 2.11, the phase of the fourth chip interval remains constant for the code value of 0. Code values of 1 and -1 change the phase value by positive and negative  $\frac{\pi}{2}$  respectively, just as in the MSK waveform. But the use of 0 as a code value brings about the possibility of the phase of the CPM waveform

<sup>1</sup>CPM used in data transmission is classically thought of coming from binary antipodal data symbols [13, 14].

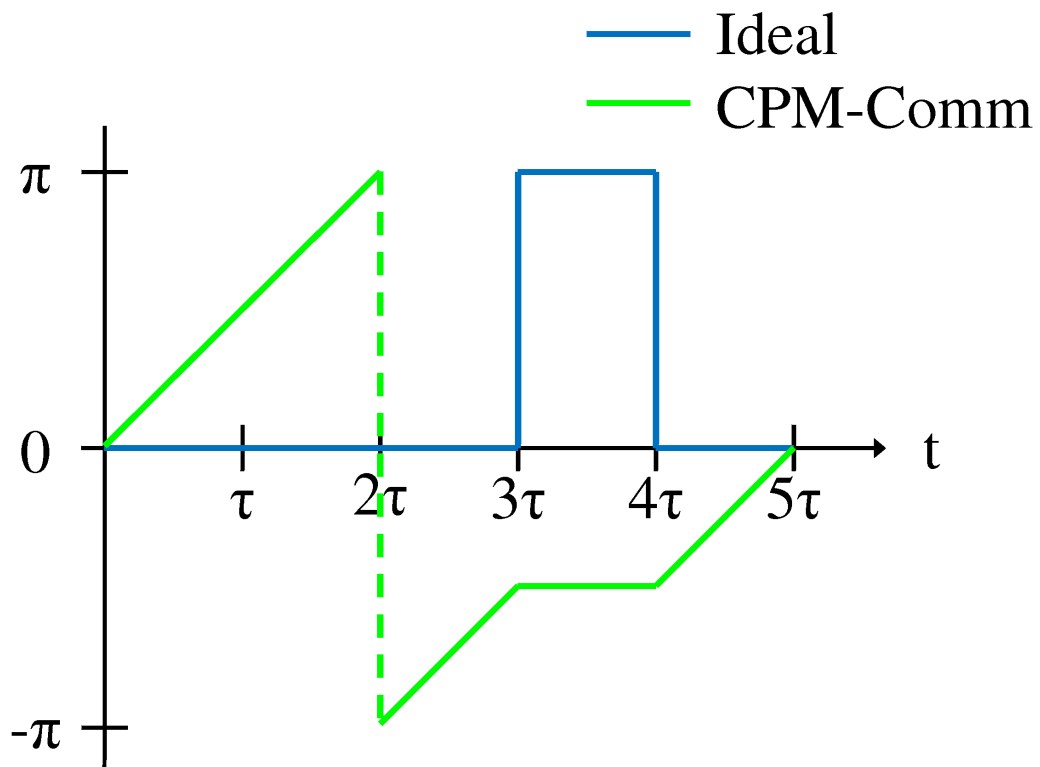


**Figure 2.15.** Phase Contrast Between Ideal Signal and CPM Signal

mimicking the phase of the Ideal waveform, which will be explored later.

Most CPM schemes are referred to by their frequency response function  $g(t)$  which is simply the derivative of the phase response function  $q(t)$ . The phase response function is defined for one symbol interval. It starts at zero and finishes at unity by the end of the interval. Its derivative, the frequency response function, will be defined over the same interval and have an integrated area of 1. Any function fitting these criteria will work as a response function. This function describes how the waveform traverses to different phase values in response to the weighted phase values  $\{\alpha_i\}$ . Many types of response have been studied, some of the more popular types include rectangular, raised cosine, and Gaussian-shaped

frequency response functions. The linear phase response function used for the plot in Figure 2.15 is implemented by using a rectangular frequency response function, which is of the form

$$g_{\text{rec}}(t) = \frac{1}{\tau} t \quad \text{for } 0 \leq t \leq \tau \quad (2.9)$$

where  $\tau$  is the duration of the chip interval.

Continuing the consideration of the length-64 MPS code, the matched filter outputs and spectral densities are compared for the CPM waveform versus the Ideal case. A rectangular filter was chosen for the frequency response shape. Figure 2.16 shows that a result similar to the MSK waveform is found for the CPM waveform for the matched filter. The normalized peak sidelobe of the CPM output is -11.4 dB, but at a chip lag of approximately 27 chips. The main lobe of the output is considerably wider, and it is evident that the sidelobe canceling properties of the binary phase code have been spoiled. If every 0 in the code is changed to a -1, as was necessary for the MSK waveform, the CPM waveform with a rectangular frequency response function is identical to the MSK waveform.

Figure 2.17 shows the PSD of the CPM waveform versus the ideal waveform, with binary values of 0 and 1 for the length-64 MPS code. A modest decrease in spectral sidelobes is shown from the MSK PSD in Figure 2.13, which employs binary values of -1 and 1 for the same MPS code. The peak of the first spectral sidelobe in the CPM waveform is at -31.6 dB, a decrease of 18 dB compared to the ideal case.

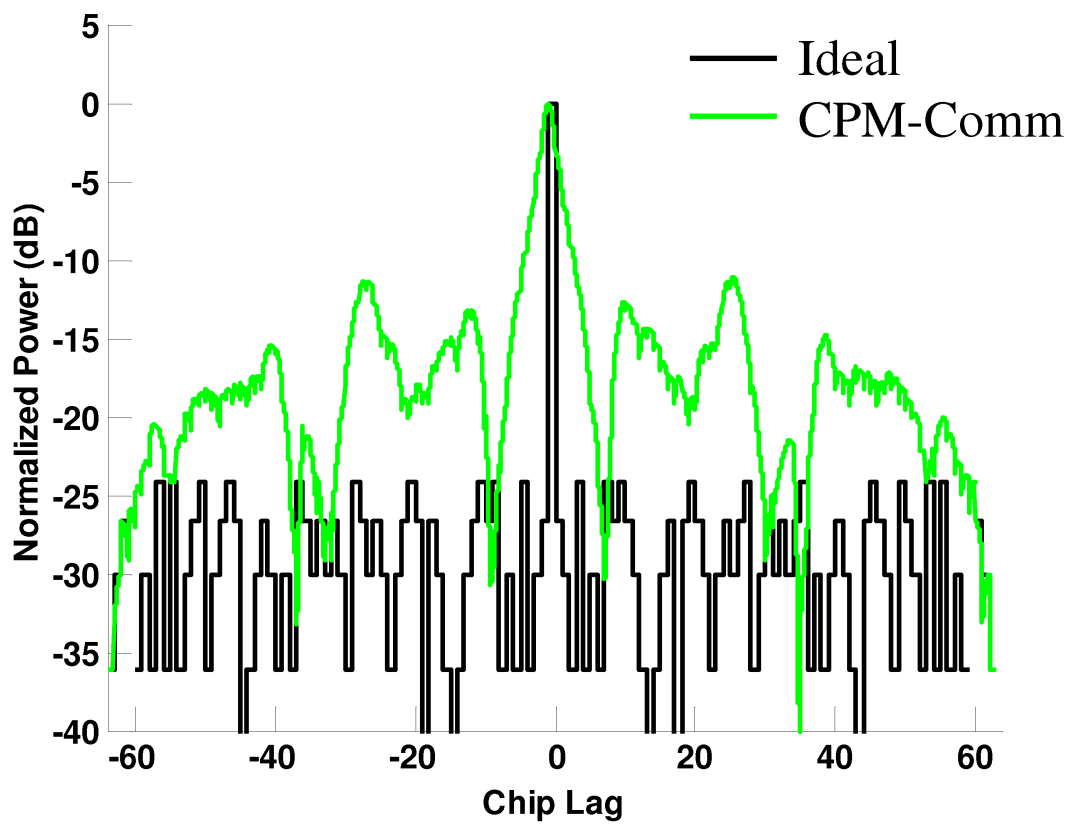


**Figure 2.16.** Receiver Matched Filter for length-64 MPS code of CPM vs. Ideal

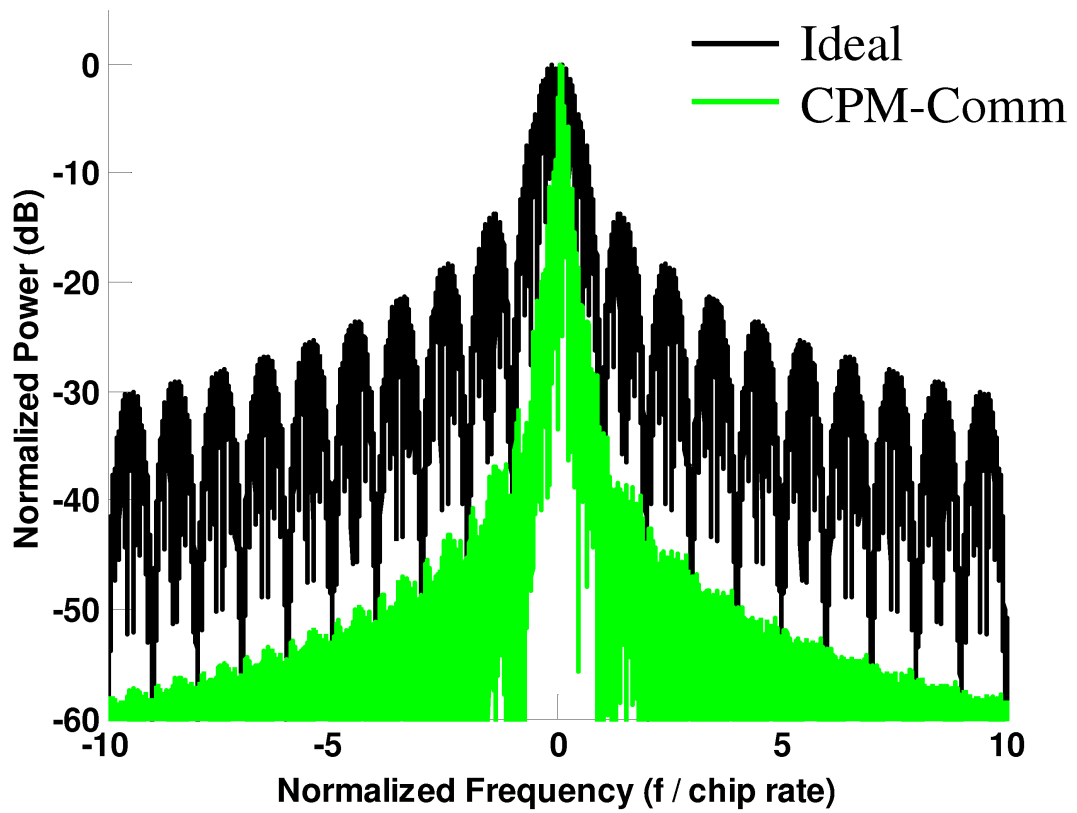


Figure 2.17. PSD for length-64 MPS code of CPM vs. Ideal

# Chapter 3

## Spectrally Efficient Implementation

The need to implement spectrally confined radar waveforms is becoming increasingly important as new multi-static and multi-access radar systems are being considered as options in the commercial and military markets. There is also need to limit spectral leakage when operating adjacent to communications bands and cooperative radar bands. There is demand for a waveform that meets spectral requirements, while retaining the desired properties of the discrete Ideal radar waveform, in particular a “small” PSL and ISL.

In this chapter a new CPM structure is proposed as a solution to reduce the spectral bandwidth of the radar waveform, while attempting to maintain the range resolution provided for a given radar code. Since the symbol modulation and other parameters important to the communications brand of CPM do not function for the radar model, a new method of encoding and generation will be needed. An additional asset gained by choosing CPM is the ability to implement polyphase radar codes, which will be shown to be a desirable property.

### 3.1 Radar CPM Model

To cast (2.7) in terms useful to radar signal processing, the  $2\pi$  value and modulation index  $h$  can be combined with the symbol value to represent a phase value in radians for some particular interval. The radar model function for a CPM waveform is

$$s(t) = \sqrt{2} \cos \left[ \omega_0 t + \sum_{i=0}^n \alpha_i q(t - iT) \right], \quad nT < t < (n+1)T. \quad (3.1)$$

This model shows a convenient method for implementing radar phase codes used in pulse compression. The phase response function  $q(t)$  can be any function that has an initial value of 0 for  $t = 0$ , and a final value of 1 at the end of one chip interval, at time  $t = T$ . An arbitrary phase code can be chosen to form a set of phase values denoted as symbols,  $\alpha_n$ , each of which is modulated onto the phase response function time shifted by  $nT$ . The block diagram of the new radar model of CPM is shown in Figure 3.1.

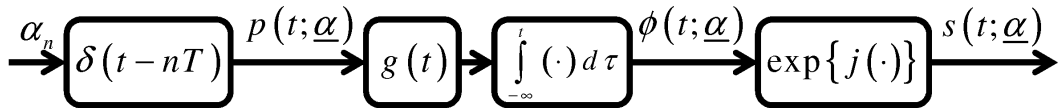


**Figure 3.1.** Radar CPM Block Diagram

Selection of the symbols  $\alpha_n$  can be accomplished by one of two different methods. The first method is to choose the symbols to be the phase values of the code. In this case the phase of the modulated waveform will transition by the amount specified by code values. This results in a condition unlike the Ideal case, where the code value is the phase value of the baseband waveform for the corresponding

chip interval. Instead, the phase transitions from the ending phase of the previous interval by the amount of the code value. This was evident in Figure 2.15. The transition occurs over the duration of the chip interval following the shape of the phase response function. A disadvantage to this method is that when the received signal is filtered, there are less cancellations at shifts away from the matched point, which leads to increased sidelobes.

Alternative to the previous method, a new symbol definition is needed to map the phase code into symbols that would modulate the phase of the resulting waveform in such a way that it is similar to the discrete Ideal waveform. This can be accomplished by making the symbol values the differential of the phase code values. This new mapping of symbol values is

$$\alpha_n = \begin{cases} \tilde{\alpha}_n & \text{if } |\tilde{\alpha}_n| \leq \pi \\ \tilde{\alpha}_n - 2\pi \cdot \text{sgn}(\tilde{\alpha}_n) & \text{if } |\tilde{\alpha}_n| > \pi \end{cases} \quad (3.2)$$

where

$$\tilde{\alpha}_n = x(n) - x(n-1) \quad \text{for } n = 1, \dots, N-1 \quad (3.3)$$

and  $\text{sgn}(\cdot)$  is the “sign” operator. The decision in (3.2) is necessary to avoid phase shifts greater than  $\pi$ . Considering the length-5 Barker code, a comparison is made of the phase of CPM waveform (with the differential symbols described in (3.2)) to the Ideal waveform, which is shown in Figure 3.2. This new form of CPM will be denoted as “CPM-Radar” while being compared to the general communications model, CPM-Comm. Comparing the CPM phase trajectories in Figures 2.15 and 3.2, it is evident that the differential CPM symbols come much closer to following the phase trajectory of the Ideal waveform than the communications model does. There is still a considerable amount of the chip interval where the phase is quite

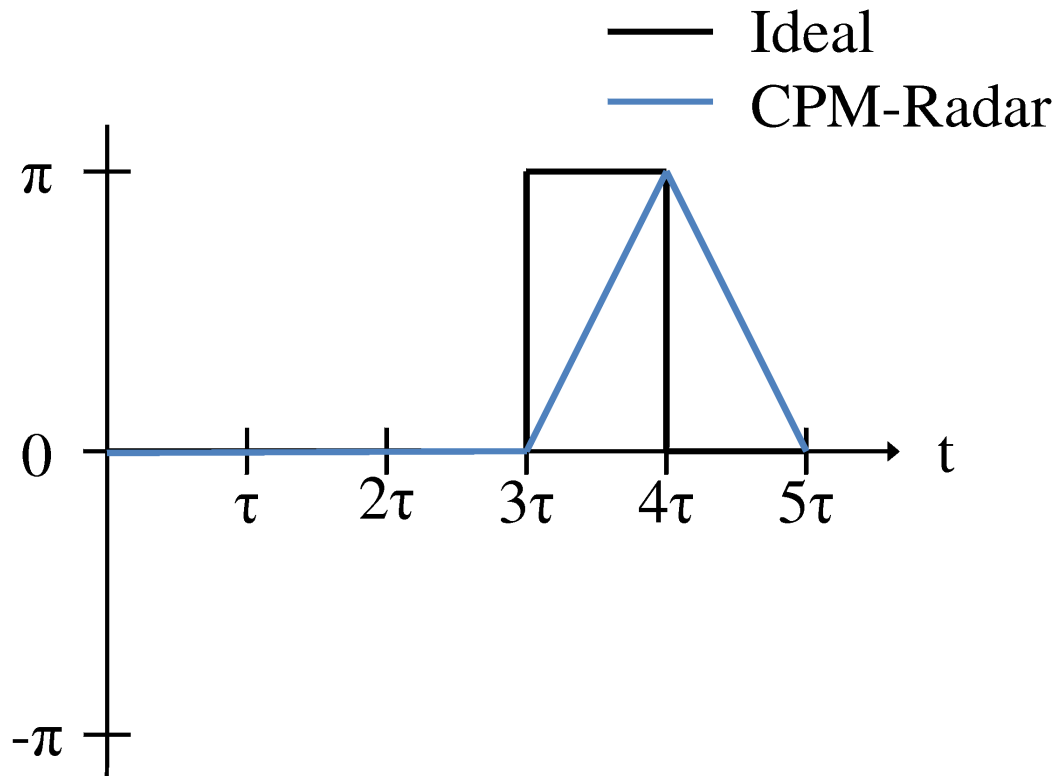


**Figure 3.2.** Phase Contrast Between Ideal Signal and CPM Signal with Differential Symbols

different than the Ideal for the CPM-Radar. Nevertheless, the general shape of the Ideal phase trajectory is achieved.

Now the Ideal and CPM-Radar receiver matched filter outputs should be compared to determine if the time sidelobe structure has improved. The length-64 MPS binary code will be considered again, as will the rectangular frequency response filter. The comparison is shown in Figure 3.3. The previous result from Section 2.5 (CPM-Comm) is plotted as well for clarity. The peak sidelobe for the new differentially encoded symbols has decreased to -14.4 dB, a modest improvement of 3 dB with respect to the communications model CPM receiver matched

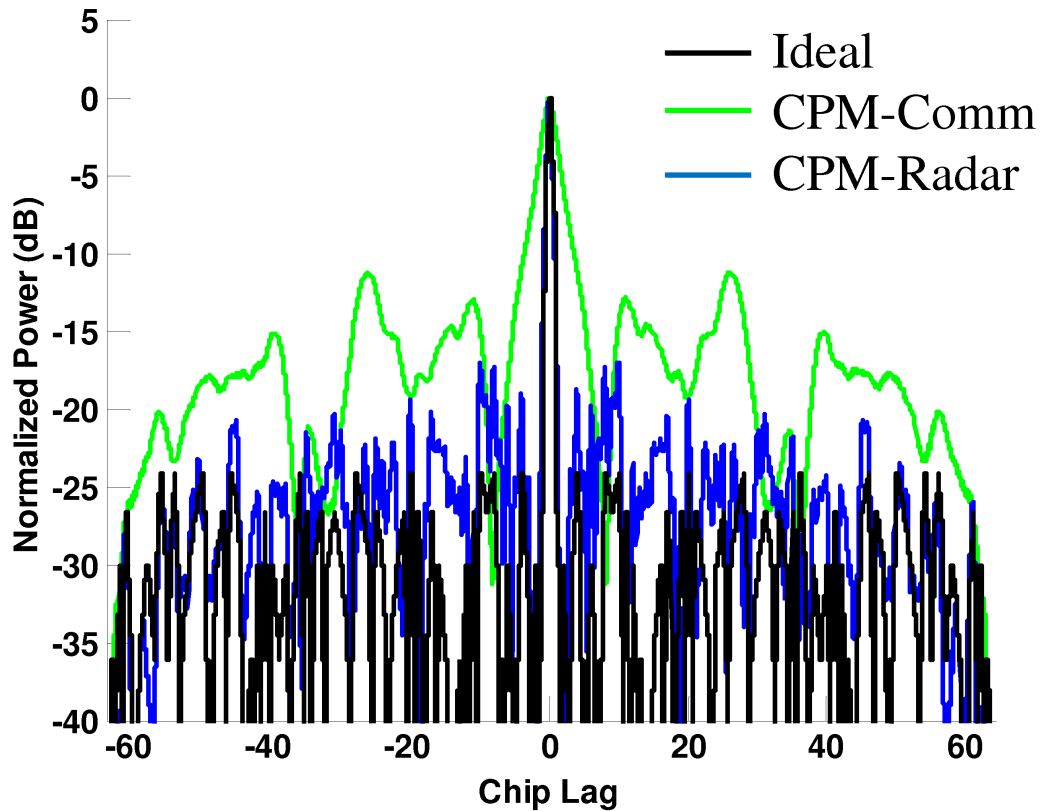


**Figure 3.3.** Receiver Matched Filter Outputs for Ideal, Communications CPM, and Differential CPM Waveforms

filter output. But the greatest improvement is in the width of the mainlobe. The distance to the first null in the general communications model is at a lag of 8 chips with respect to the peak. The distance for the differential case is 2 chip lags with respect to its peak, which is the same distance for the ideal output. Also note that the integrated sidelobe level (ISL) has decreased considerably.

The power spectral density of CPM-Radar must also be considered. This comparison is shown in Figure 3.4. The spectral sidelobes have increased for the differentially encoded CPM waveform with respect to the communications CPM waveform. Also, there are large spikes present, located harmonically at spacings

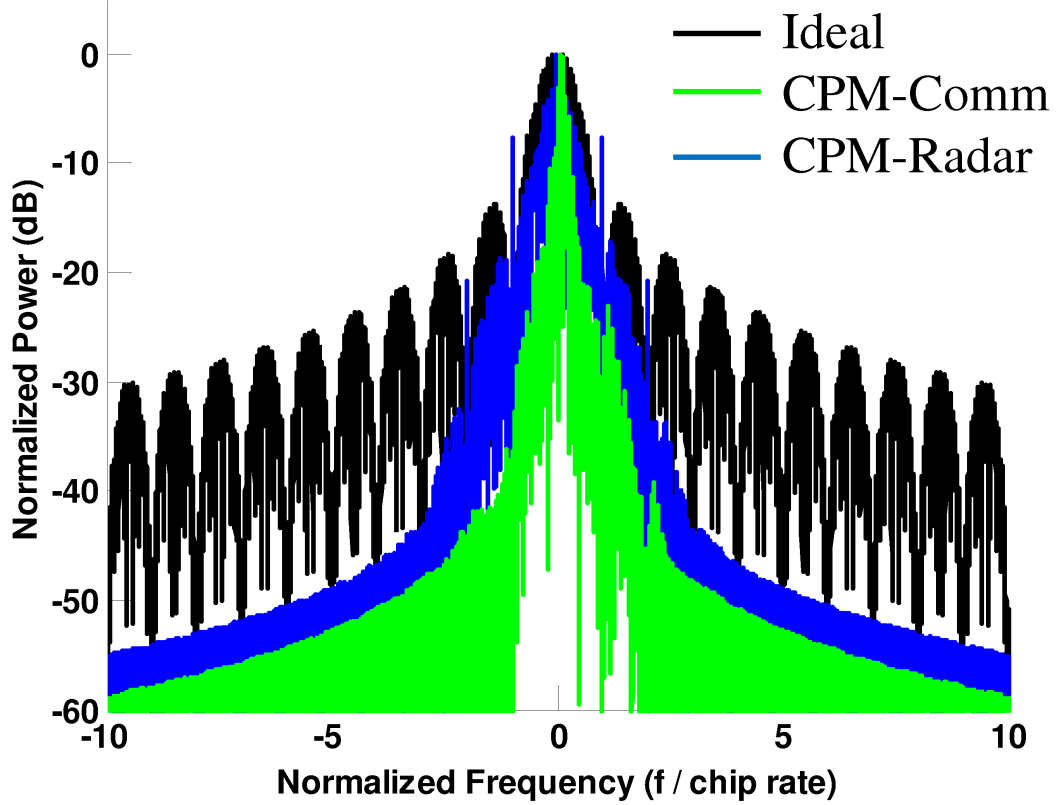


**Figure 3.4.** PSD for Ideal, Communications CPM, and Radar CPM Waveforms

equal to the chip rate. The phase shifts in the communications case are either positive phase shifts of  $\frac{\pi}{2}$  or no phase shift, because the symbols are from the binary code  $\alpha_n \in \{0, 1\} \Rightarrow \{0, \frac{\pi}{2}\}$ . However, the phase shifts in the CPM-Radar model come from differentially encoded symbols  $\alpha_n \in \{-\pi, 0, \pi\}$ . This is evident in a plot of the unwrapped phase shown in Figure 3.5. The phase of CPM-Radar appears to be an inverted likeness of the Ideal waveform's phase. The major difference is that CPM moves to the phase values at  $-\pi$  by traversing clockwise, and the Ideal waveform transitions instantaneously to  $+\pi$ , which of course is the same angle as  $-\pi$ . The phase trajectory of CPM-Comm waveform shows a

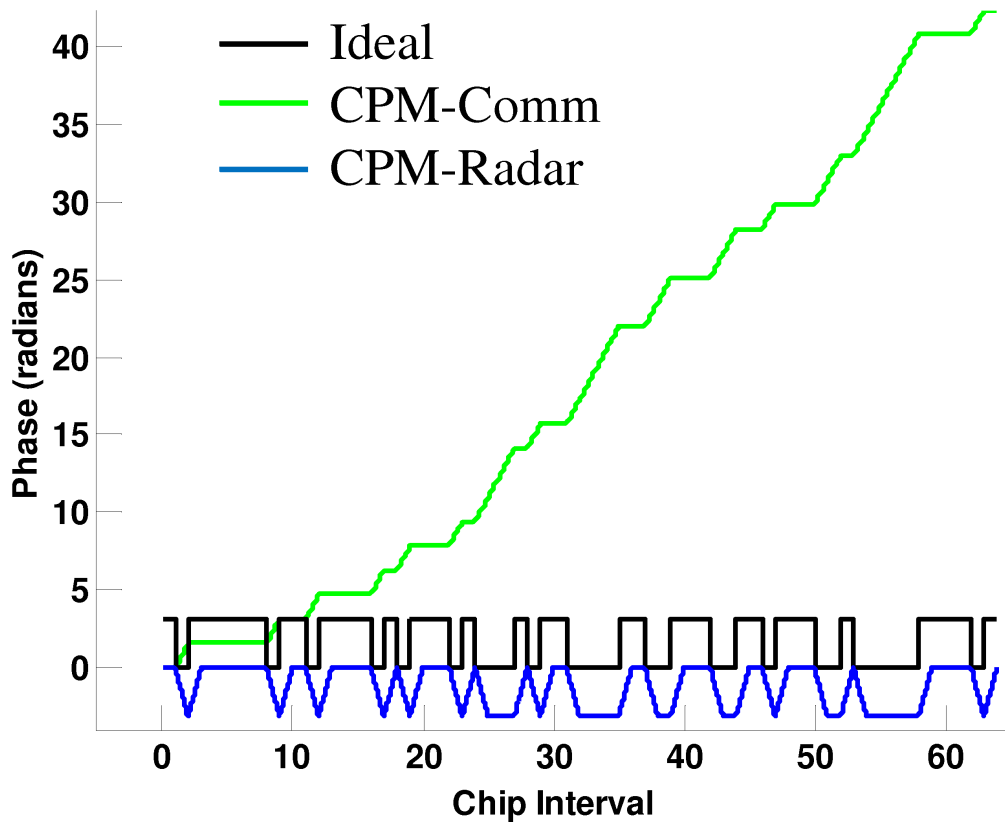


**Figure 3.5.** Unwrapped Phase for the General CPM and Differential CPM Waveforms

monotonically increasing phase, increasing at most  $\frac{\pi}{2}$  in a single chip interval.

The results of Figure 3.3 indicate that it is logical to proceed with the differential symbol encoding for the CPM-Radar model over the direct method used in the general CPM model. The dynamic range has been greatly increased with a penalty of increased spectral power. Perhaps changing the frequency response function to one that smooths the abrupt changes in the phase trajectory could alleviate some of this increase. This could be accomplished with the raised cosine

filter in place of the rectangular filter. The formula for the raised cosine filter is

$$g_{\text{RC}}(t) = A \left( 1 - \cos \left( 2\pi \frac{t}{\tau} \right) \right) \quad \text{for } 0 \leq t \leq \tau \quad (3.4)$$

where  $A$  is a normalizing constant, which in this case should be set to give the filter a total area of unity because all weighting of the phase increase comes directly from the phase code. The effect of this filter decreases the slope of the phase (*i.e.* frequency) so that the majority of the spectral spreading is not due to instantaneous changes in frequency. Stated another way, the phase function of the waveform will be second-order differentiable.

In [10], two types of continuous phase shift modulations (CPSM) are defined, these are minimum shift keying (MSK) defined in Equation 2.6 and derivative phase shift keying (DPSK) defined in Equation 2.2. These modulation types make good comparison waveforms for spectral efficiency and suppression of range sidelobes when considering binary waveforms. A benefit of CPM over DPSK and MSK is that in addition to the available binary codes, polyphase codes are now an option for code selection. However, DPSK and MSK can no longer make direct comparisons. For a polyphase radar code, the mapping in (3.2) and (3.3) predict phase shifts  $\leq |\pi|$ . So for some of the phase shifts in the code, the shift is smaller than  $\pi$ , but over the same time interval. This will spread out the spectral energy in a more uniform manner.

### 3.2 Rise-/Fall-Time Considerations

An additional source of spectral sidelobes comes from the amplitude changes in the waveform. The radar waveform that has been proposed is a constant

modulus waveform. However, effects of turning this waveform on and off at the output of the transmitter will certainly produce spectral regrowth effects that can be addressed. Thus far the waveform has been modeled as turning on (and off) instantaneously. This would cause an increase in spectral content, so comparing the CPM waveform to others in this case could mask some of the gain provided thru CPM. A solution is needed to address these portions of the waveform denoted as the rise-time and fall-time of the waveform.

To alleviate some of the spectral problems introduced by the rise- and fall-time, the time to transition on and off must be increased to some finite duration. Further, the transition shape can be considered, effecting the overall modulus of the waveform. Two transition types will be considered here. The first is a linear transition lasting some percentage of a chip interval, ramping up for the first chip and ramping down for the last chip. This is shown in blue in Figure 3.6. The

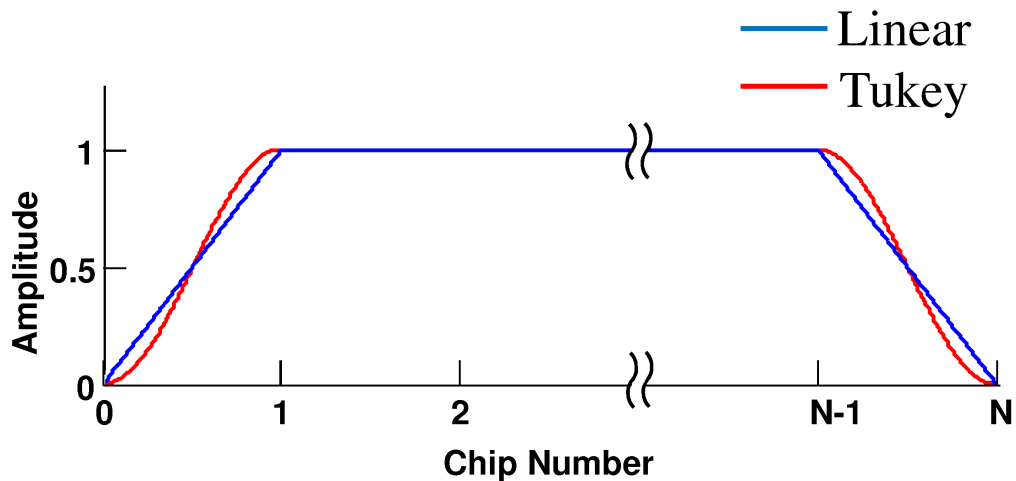


**Figure 3.6.** Two Amplitude Windows to Reduce Spectral Leakage

shape of the amplitude mask over the duration of the waveform is trapezoidal, with the greatest portion in the middle at unit modulus. The second amplitude

mask considered is a Tukey window, which is the red trace in Figure 3.6. In this case the pre- and post-amble of the waveform will be the shape of a  $\cos(\cdot)$  function. The phase of the  $\cos(\cdot)$  forms transitions from  $\pi$  to  $2\pi$  for the pre-amble, and from  $0$  to  $\pi$  for the post-amble. The time to transition to unit modulus will be the same percentage of a chip interval as used in the first case of linear transition. Without loss of generality, the transition time, on or off, will be modeled to last exactly one chip interval. So, only the first and last chips of the waveform will not be constant modulus. This is illustrated in Figure 3.6. Note the corner that is present at the two transition points at  $1$  and  $N - 1$  for the linear transitions. But at the same transitions for the Tukey window, the amplitude is smooth and continuous. The same can be said for the very beginning and end of the window. The linear window has an immediate positive and negative slope for the beginning and end of the window respectively. The Tukey window transitions smoothly from off to on and vice versa.

For the simulation of these amplitude windows, a new radar code is considered. The code that is used is a length-64 Nunn-Kretschmer code [15]. The code is listed here in Table 3.1 for easy reference. This code is designed to be paired with an optimal mismatched filter for a minimal ISL and PSL, which will be seen later. This emphasizes the added possibilities gained by having the ability to implement polyphase codes.

Using the radar code in Table 3.1, a CPM waveform was modulated and amplitude windowed with the Tukey and linear windows shown in Figure 3.6. From hence forth the CPM-Radar waveform will be referred to only as the CPM waveform, since comparison to the communications model showed that the differentially encoded model of CPM is more suited for the pulse compression/matched

**Table 3.1.** Nunn-Kretschmer Polyphase Code in Radians

Chip	Phase	Chip	Phase	Chip	Phase	Chip	Phase
1	0.000	17	-1.407	33	2.988	49	-2.346
2	-0.070	18	-3.058	34	-2.191	50	-0.062
3	0.031	19	2.292	35	0.198	51	1.651
4	-0.040	20	2.103	36	-0.046	52	-2.896
5	-0.173	21	-2.147	37	-1.803	53	-1.338
6	-0.247	22	-1.173	38	2.086	54	-0.076
7	-0.508	23	-1.358	39	0.488	55	2.351
8	-0.691	24	1.267	40	-1.333	56	0.592
9	-0.812	25	-0.778	41	-3.091	57	3.063
10	-1.086	26	0.867	42	1.013	58	-1.122
11	2.656	27	0.526	43	-1.651	59	1.702
12	2.539	28	2.790	44	0.604	60	-1.655
13	2.270	29	1.575	45	2.292	61	0.329
14	0.866	30	-2.184	46	-1.914	62	2.467
15	0.438	31	0.983	47	2.356	63	-2.347
16	-0.454	32	-0.982	48	-0.200	64	0.000

filter problem. The PSD of the two outputs is shown with the PSD of the original on/off waveform and the Ideal waveform from (2.1) in Figure 3.7. There are two profound results in examining Figure 3.7. The first is the decrease in spectral sidelobes. In fact, there is no spectral power above -60 dB outside of a bandwidth of approximately three times the chip rate for the windowed waveforms. This is significant corroboration that the amplitude transitions of the radar waveform have a huge impact on the PSD of the waveform. The second profound result is that there is minimal difference between the linear and Tukey windowed waveform PSDs. This result suggests that perhaps some arbitrary, smooth, nonlinear transition shape could be used with minimal impact on the significant gain achieved in spectral containment. Such would be the case in controlling high power nonlinear radar amplifiers for longer time intervals in the nonlinear region.

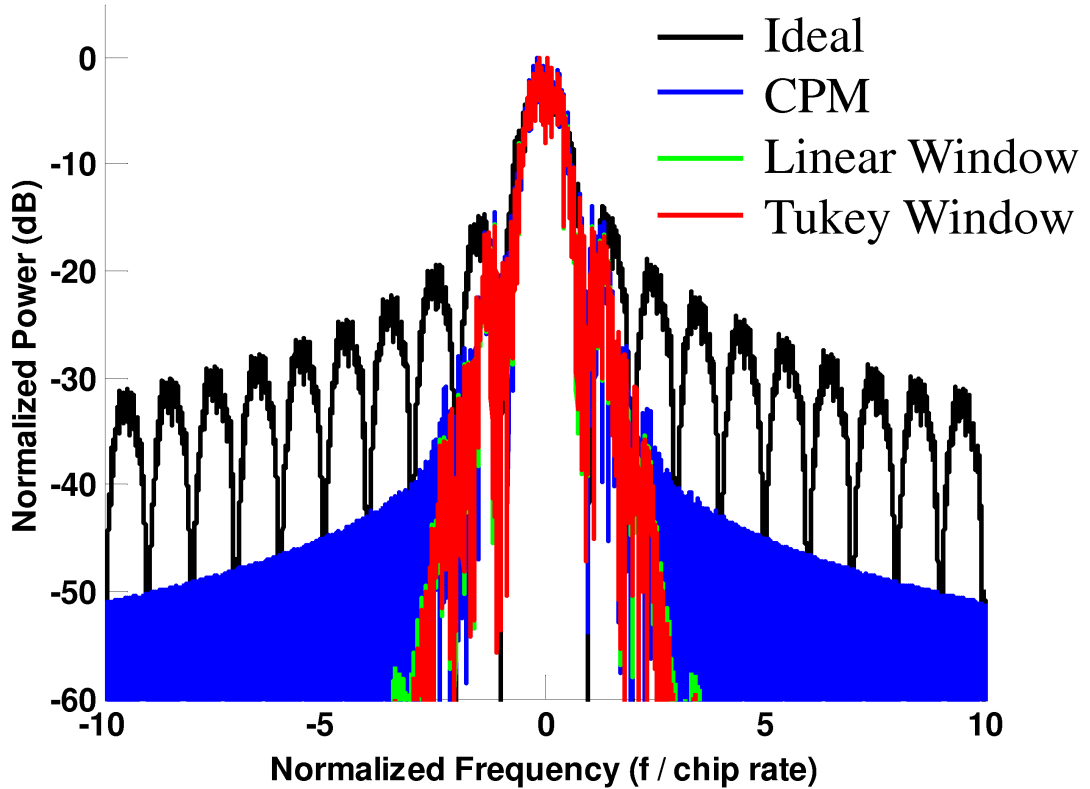


**Figure 3.7.** PSD of Ideal, “On/Off” CPM, and CPM Windowed Waveforms

To illustrate the power loss associated with the filter, consider the simple case of the linear window with the transition over one chip interval, on a length-100 phase coded waveform with a 10 nanosecond chip interval transmitted on a radar with 100 megawatts of peak power. This would result in a 1 microsecond waveform, with a total energy of 1 joule for the “on/off” case. Each chip contributes 0.01 joules of energy, and a linear transition across the chip interval would result in  $\frac{1}{4}$  the chip energy of the square shape. The total power loss incurred from windowing this case is

$$P_{\text{lost}} = 1 \text{ J} - (98 \cdot 0.01 + 0.25 \cdot 2 \cdot 0.01) \text{ J} = 0.015 \text{ J}. \quad (3.5)$$

So in this simple example, a total power loss of only 1.5% has been incurred. This indicates it would be beneficial to take the loss in power for the decrease in spectral regrowth, which is much more significant. This could be compensated by increasing the transmitter peak power a modest 1.5 megawatts to 101.5 megawatts.

Now as a second check, the PSD of the DPSK and MSK waveforms amplitude weighted with a Tukey window need to be compared to the Tukey windowed CPM waveform. Deviations from the Tukey taper have been found to cause little change in the spectral content as long as the rise/fall-time each occurs over the duration of the chip interval  $\tau$ . To achieve this effect, a method has been proposed of shifting two waveforms 180° out-of-phase by 90° in opposite directions over the duration of the pulse rise-time so that they are in-phase. Then the waveforms are shifted back 180° out-of-phase during the pulse fall time. This method is called Chireix out-phasing and is discussed in [10, 16, 17].

Figure 3.8 shows that CPM still offers significant benefit over MSK and DPSK with respect to spectral sidelobes. Due to the binary code limitations of MSK and DPSK, the length-64 MPS code that was used to generate the PSDs of Figures 2.10, 2.13 and 2.17 in Chapter 2 was used here to highlight the improvement of using a window for the same code and same waveform parameters. Very little improvement is seen for the Ideal waveform. Spectral sidelobes that might not appear because of instantaneous amplitude shifts are still occupied with sidelobes from instantaneous phase shifts. DPSK shows some improvement out at the higher frequencies but maintains the same shape within a bandwidth of four times the chip rate. The definition of bandwidth for a baseband waveform used here includes the sum of positive and negative frequencies centered at zero, since the waveform will certainly be mixed to a radio frequency. MSK has significant improvement

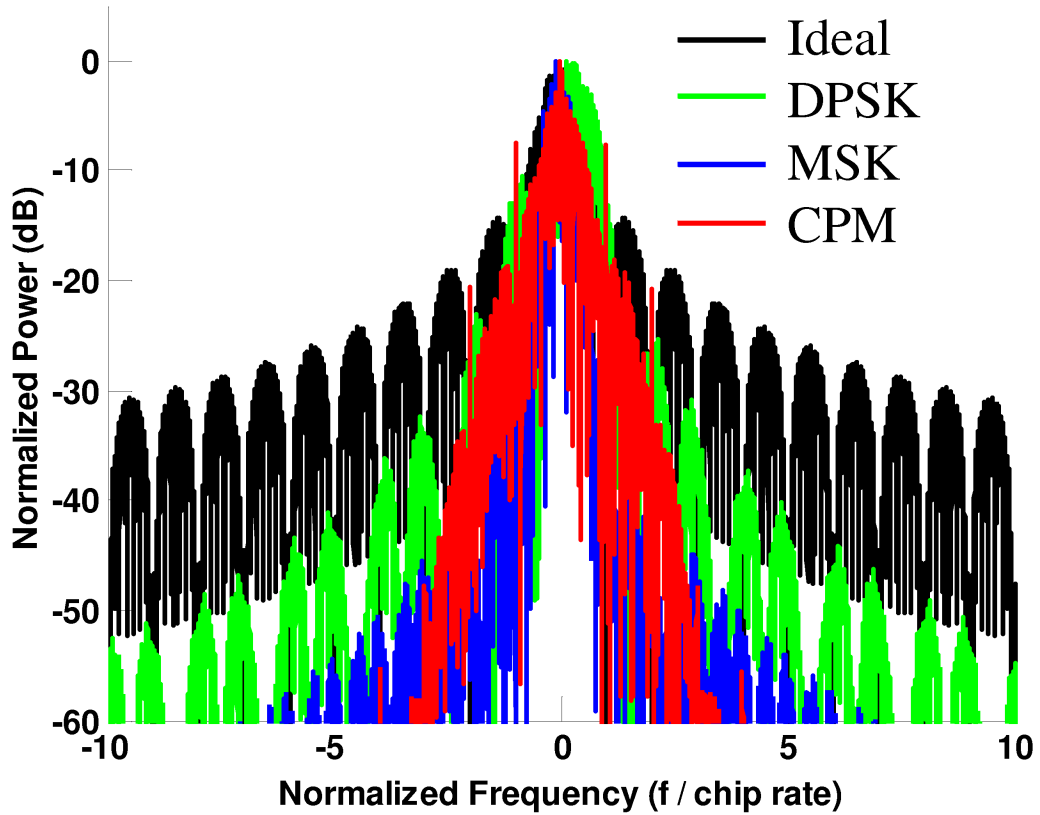


**Figure 3.8.** PSD of Ideal, DPSK, MSK, and CPM Tukey Windowed Waveforms

for frequencies whose magnitude is greater than two times the chip rate. But CPM has dramatic improvement. There are no spectral sidelobes with normalized power greater than -60 dB outside a bandwidth of 8 times the chip rate. Note that there are still sharp peaks located at harmonics of the chip rate for the CPM waveform modulated under the radar framework (these peaks are not present in the communications model of the CPM modulator used in Figure 2.17). This further confirms that this could be a product of the  $0$  to  $\pi$  modulation in the binary case.

Upon examining Figures 3.7 and 3.8, it is evident that a radar implementation

of CPM can offer significant spectral benefits with respect to some current methods used. The benefit for CPM is even greater because it can support polyphase codes, which means more codes of longer length. The obstacle that must be overcome is range sidelobes. The smooth shape and reduced bandwidth of CPM induces an increased PSL and ISL in the filtered output of the received signal. To address this, a different filter type is introduced in Chapter 4 as an alternative to the matched filter considered up until now.

## Chapter 4

# Receive Filter Implementation

Now that it has been established that the CPM framework offers a decrease in spectral spreading, the issue of receive filtering must be addressed to determine what is necessary to achieve a “good” radar output after receiver filtering. Namely, a sufficiently low PSL and ISL, and an acceptable range resolution with regards to mainlobe width must be met in order for the spectrally contained radar waveform to be considered practical. One consideration is that the chip duration can be shortened to increase range resolution, at the cost of trading back some of the gain achieved in spectral containment. Even though, a stringent spectral mask can be met while efficiently using the prescribed bandwidth. The Doppler resolution can be increased by using longer codes which are available because polyphase codes can be used.

Broadly speaking, there are two filter categories to apply to the received signal. These are the matched filter and the mismatched filter. The matched filter provides the maximum SNR, which is certainly desirable in a radar output. However, the matched filter does not generally provide the lowest peak sidelobes and integrated sidelobes (ISL and PSL). If the noise power is less than power of the

output sidelobes, a small decrease in SNR would be insignificant if the PSL could be greatly increased. A mismatched filter peak receiver output will be slightly less than the matched filter receiver output at the matched point, thus a degradation in SNR is incurred. But if a significant decrease in PSL and ISL is attained, the dynamic range can be greatly improved with no penalty from the decreased SNR as long as the noise power is less than the maximum sidelobe power.

## 4.1 Matched Filter

When applying the matched filter in simulation, the structure of the filter needs to be defined in order to account for the degree of oversampling in the digitized return waveform. The waveform will be highly sampled in the transmitter as it is applied with a digital arbitrary waveform generator (DAWG). The high degree of oversampling allows a smooth, continuous-time waveform to be launched from the antenna. When the target reflection is received the samples in the receiver will not be taken as close as they were presented in the transmitter, but there will still be multiple samples per chip. The matched filter is defined as

$$g_{\text{MF}}(n) = x_r^*(-n) \quad (4.1)$$

where  $x_r(n)$  is the digitized received waveform,  $n$  is the sample index and  $*$  denotes the complex conjugate operator. Consider the simple case of a single point scatterer where the received waveform is exactly one reflection of the transmitted waveform and the sampling rates are the same. The output of the filter is then

$$y(l) = x_r(n) * g_{\text{MF}}(n) = \sum_{n=-\infty}^{\infty} x_r(n) \cdot x_r^*(l+n) \quad (4.2)$$

which is the equation for the autocorrelation of a digital waveform. But now let the matched filter have samples spaced by some portion of the chip interval  $\tau$  with zero filling to achieve a sample rate equal to that of the received waveform. If one sample is used per chip interval, the filter is referred to as the nominal matched filter. In this case each element from the code is taken in reverse order, then conjugated and spaced with zero valued samples by equal time intervals of the chip duration  $\tau$ . The filter has the comb shape shown in Figure 2.4 and was first used for plot shown in Figure 2.3, and is the same filter used for the results found in Figure 3.3.

## 4.2 Mismatched Filter

The implementation of the comb structured matched filter can be easily extended to a longer mismatched filter, or any other “low sidelobe” receive filter structures such as Adaptive Pulse Compression [18]. The particular structure treated here is the Least Squares based mismatched filter [19]. First the pulse compression matrix is formed as

$$\mathbf{A} = \begin{bmatrix} \mathbf{s} & 0 & \cdots & 0 \\ 0 & \mathbf{s} & \ddots & \vdots \\ \vdots & \ddots & \ddots & 0 \\ 0 & \cdots & 0 & \mathbf{s} \end{bmatrix} \quad (4.3)$$

which is of dimension  $(N + M - 1) \times M$ .  $M$  is typically some multiple of  $N$  on the order of 1 or 2 and  $\mathbf{s}$  is the  $N$ -length code with the  $n^{th}$  element defined as

$$\mathbf{s}_n = e^{jx(n)}. \quad (4.4)$$

Note that (4.4) is just a vector of complex amplitudes for each corresponding phase element taken directly from the radar code, and  $N$  is the number of elements in the code. Using (4.3) the LS matrix is

$$\mathbf{\Phi} = (\mathbf{A}^H \mathbf{A})^{-1} \mathbf{A}^H. \quad (4.5)$$

where  $(\cdot)^H$  is the hermitian operator denoting a matrix conjugate transpose. The LS-based mismatch filter can be calculated by

$$\mathbf{h}_m = \mathbf{\Phi} \mathbf{e}_m \quad (4.6)$$

where  $\mathbf{e}_m$  is a  $(N + M - 1)$ -length elementary vector of all zeros with the exception of the  $m^{th}$  element which has a value of 1. The purpose of the elementary vector is to extract a single column from  $\mathbf{\Phi}$  to be used as a filter. Each column is a shifted copy of the adjacent columns, except for the outer  $(N - 1)$  columns where clipping occurs. Generally  $m$  is selected around  $\frac{(N+M-1)}{2}$  so that the filter comes from the middle of  $\mathbf{\Phi}$ . This filter structure, based on one sample per code element, will be referred to as the nominal mismatch filter.

Taking advantage of the polyphase capabilities of the CPM framework, the length-64 Nunn-Kretschmer code from Table 3.1 will be used for analysis. Remember that this code was specifically designed for use with a mismatch filter as is detailed in [15]. The results of the receiver mismatch filter output using the nominal mismatch filter are presented in Figure 4.1. Note that the mismatch filter output has more shifts than the output for the matched filter. This is because the mismatch filter is longer than the matched filter by a factor of  $M$  for this case. Alignment of the peak will be dependent upon the choice of  $m$  in the elementary

vector, which has been centered at zero here for clarity. The PSL for the Ideal

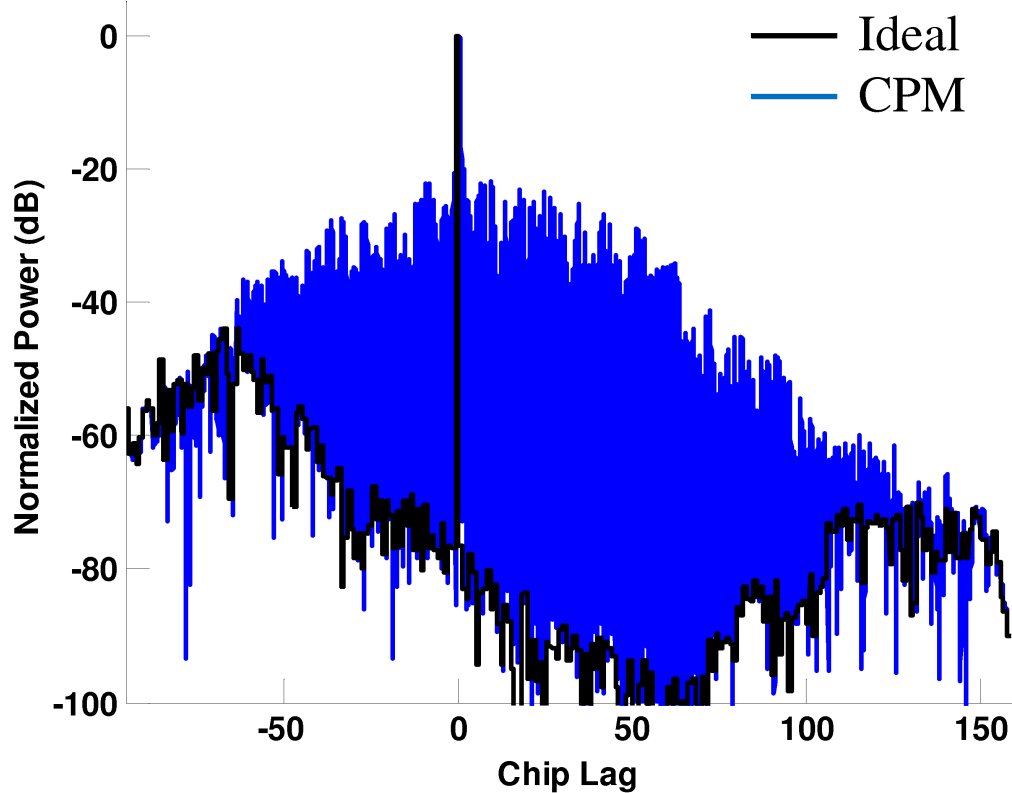


**Figure 4.1.** Ideal and CPM Receiver Mismatch Filter Output for length-64 Nunn-Kretschmer code

waveform is  $-43.9$  dB, where for the CPM waveform it is only  $-19.95$  dB. This significant difference in range resolution can be attributed to the transitioning phase of the CPM waveform. The Nunn-Kretschmer code, specifically optimized under the assumption of the infinite bandwidth Ideal waveform described by (2.1), performs beautifully when the phase code value is held constant throughout the chip interval. It is evident that this approach using the nominal number of elements for the LS formulation is insufficient. There is simply too much information lost describing the phase transition that occurs over the chip interval for the CPM

waveform. For this reason an over-sampled formulation of the LS-based mismatch filter is needed to account for this additional complexity.

Define a new vector taken from  $NK$  evenly spaced samples of the CPM waveform from (3.1) and denote it as  $\mathbf{s}_{\text{CPM}}$ .  $K$  is the oversampling factor that sets the number of samples per chip interval to be used. A value of  $K = 1$  corresponds to 1 sample per chip such as employed in the nominal mismatch filter framework. Using this length- $NK$  oversampled waveform in (4.3) the new pulse compression matrix is defined as

$$\mathbf{A}_{\text{CPM}} = \begin{bmatrix} \mathbf{s}_{\text{CPM}} & 0 & \cdots & 0 \\ 0 & \mathbf{s}_{\text{CPM}} & \ddots & \vdots \\ \vdots & \ddots & \ddots & 0 \\ 0 & \cdots & 0 & \mathbf{s}_{\text{CPM}} \end{bmatrix} \quad (4.7)$$

which has dimensions  $(NK + M - 1) \times M$ . The new LS-based mismatch filter can then be obtained as

$$\mathbf{h}_m = (\mathbf{A}_{\text{CPM}}^H \mathbf{A}_{\text{CPM}} + \delta \mathbf{I})^{-1} \mathbf{A}_{\text{CPM}}^H \mathbf{e}_m. \quad (4.8)$$

where  $\mathbf{I}$  is the identity matrix and  $\delta$  is a loading factor. The diagonal loading term  $\delta \mathbf{I}$  is necessary because the over-sampled waveform  $\mathbf{s}_{\text{CPM}}$  results in  $(\mathbf{A}_{\text{CPM}}^H \mathbf{A}_{\text{CPM}})$  being ill-conditioned. The result of this receiver mismatch filtering using the over-sampled filter defined in (4.8) is shown in Figure 4.3. The code being considered is the length-64 Nunn-Kretschmer code used before. A loading factor of  $\delta = 10^{-0.14}$  was used for the mismatch filter calculation. This value of delta was found by examining the eigen-spectrum of the pseudo-inverse argument  $(\mathbf{A}_{\text{CPM}}^H \mathbf{A}_{\text{CPM}})$  which is shown in Figure 4.2. A “knee” was seen at a value of  $-1.4$  dB, therefore this

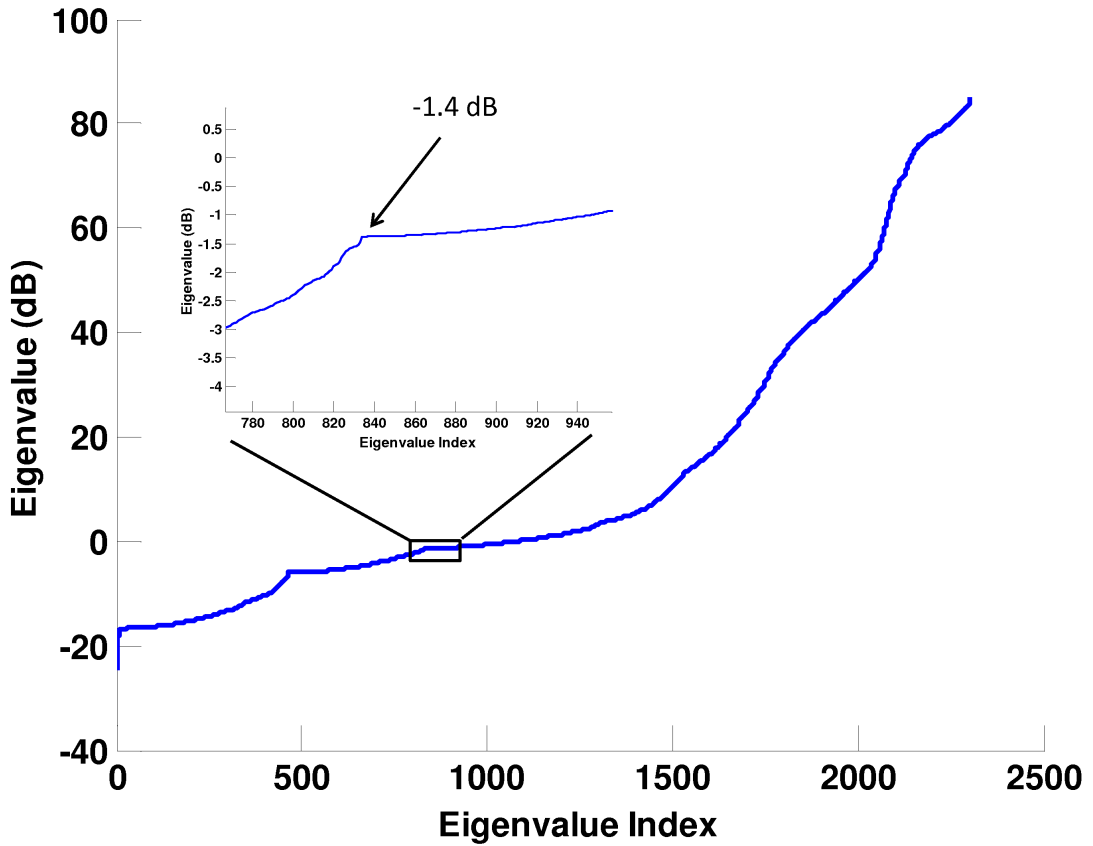


**Figure 4.2.** Eigen-Spectrum of  $(\mathbf{A}_{\text{CPM}}^H \mathbf{A}_{\text{CPM}})$  Using length-64 Nunn-Kretschmer code with  $K = 10$

value was chosen as the loading factor. This value works well for all CPM waveforms considered in this work but cannot be considered optimal. The choice of loading factor is rather arbitrary as long as it is outside of the obvious “signal subspace”, which lies approximately to the right of index 1500 in Figure 4.2. A Tukey window amplitude taper has been applied to the waveform. This builds in a more realistic case of a finite transition time, as opposed to the square transition that would require infinite power. The window also helps to smooth results by attenuating components at the ends of the waveform as their contribution drops off from the compression of the pulse. The normalized peak power is approxi-

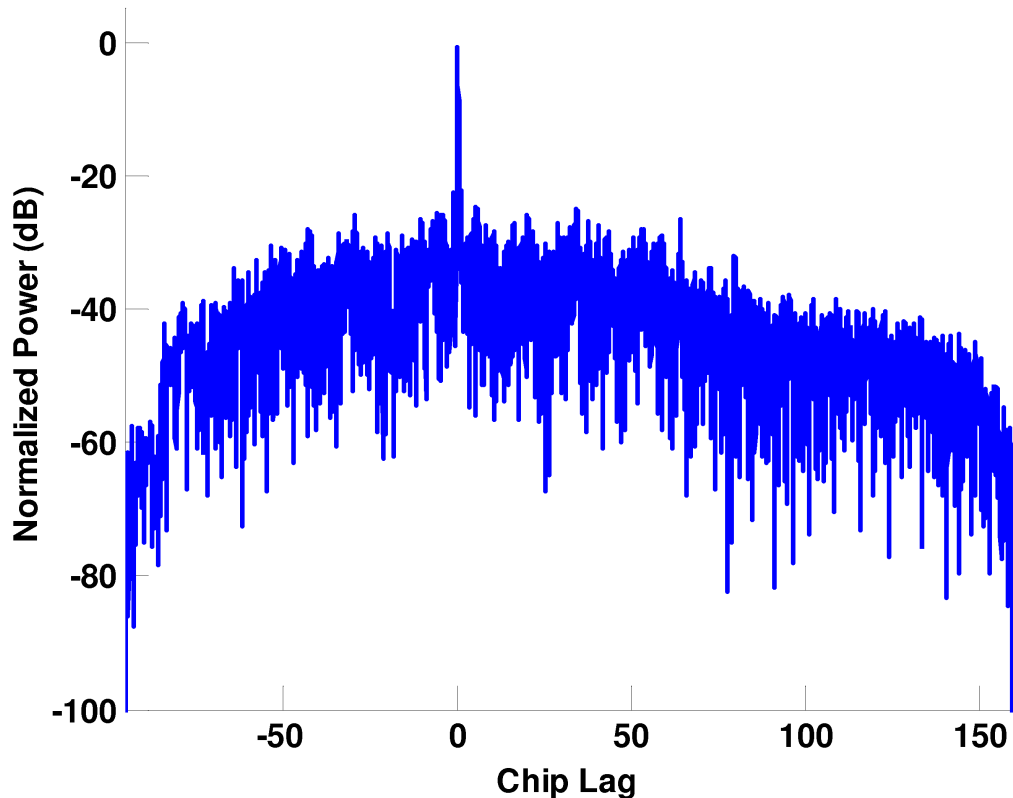


**Figure 4.3.** CPM Receiver Mismatch Filter Output Using length-64 Nunn-Kretschmer code with  $K = 10$

mately -0.6 dB relative to the non-windowed receive matched filter output. The normalization is based on the compression gain resulting from matched filtering, so the result of a peak power less than 0 dB is attributed to mismatch filter loss, or just mismatch loss. Thus, in this case the mismatch loss is about 0.6 dB.

It is not immediately evident in Figure 4.3 how much the added information built into the LS-formulation has contributed. The PSL for this CPM waveform is approximately -22 dB, in close to the peak at a lag of 1.1 chips. This is a slight improvement of 2 dB from the nominal case. The overall sidelobe structure appears more uniform than what was seen in Figure 4.1. But to see another benefit, a zoomed in look at the peak is shown in Figure 4.4. The peak sidelobes

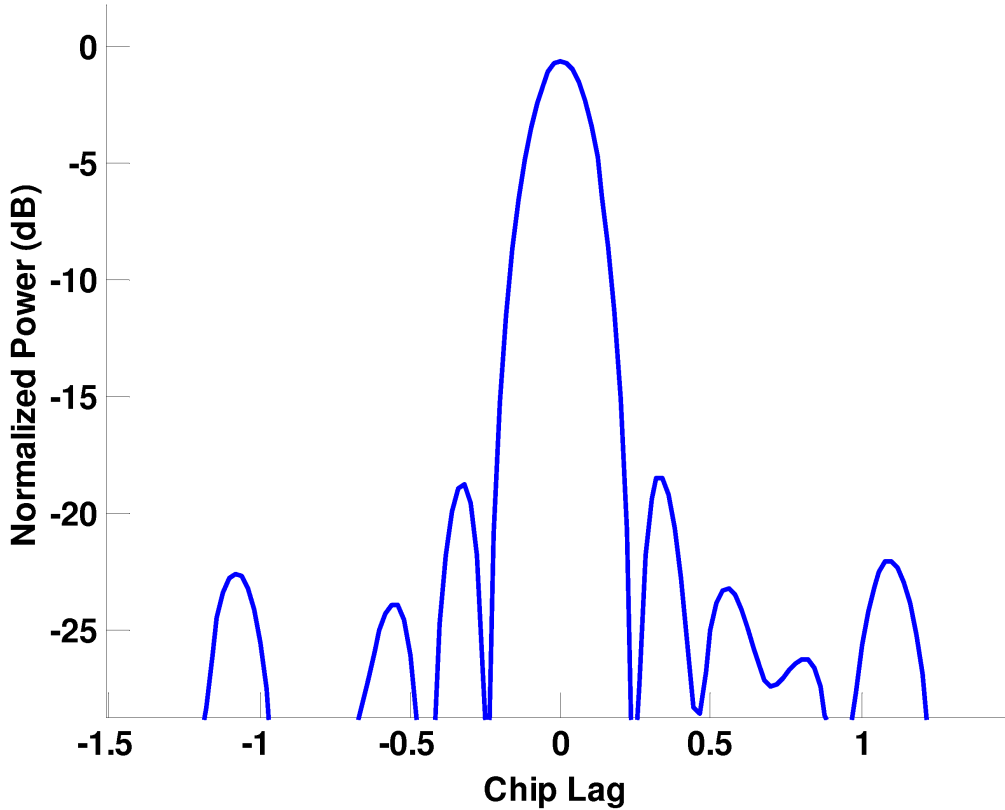


**Figure 4.4.** CPM Receiver Mismatch Filter Output Using length-64 Nunn-Kretschmer code with  $K = 10$

are just outside  $\pm 1$ , and the envelope of the main lobe is approximately between  $\pm 0.5$ . Note how the first null occurs around a lag of  $\pm 0.25$ . The resolution of the main lobe is less than half of a chip width at a level of -18.5 dB above the closest two lobes, if they are excluded from the main lobe envelope. This benefit is a direct result from the over-sampled formulation in (4.8) referred to as range super-resolution. Further discussion of this topic can be found in [18].

A well-known approach to trade resolution for reduced range sidelobes for the LS-based mismatch filter formulation is to remove rows of  $\mathbf{A}_{\text{CPM}}$  surrounding the  $m^{\text{th}}$  row. It would be desirable to decrease the sidelobes as much as possible, to

a point where the nominal resolution is achieved. To accomplish this,  $\frac{K}{2}$  rows above and below the  $m^{\text{th}}$  row were removed from  $\mathbf{A}_{\text{CPM}}$ . Then  $\mathbf{h}_m$  is calculated as before.

Continuing analysis of the CPM waveform used in Figure 4.4 based on the length-64 Nunn-Kretschmer code with  $K = 10$ , the result of the receiver mismatch filtering is shown in Figures 4.5 and 4.6. Both figures are of the same result, only that Figure 4.6 has been zoomed in on the mainlobe and includes the two peak sidelobes. The resolution spoiling trade-off successfully decreases the sidelobes

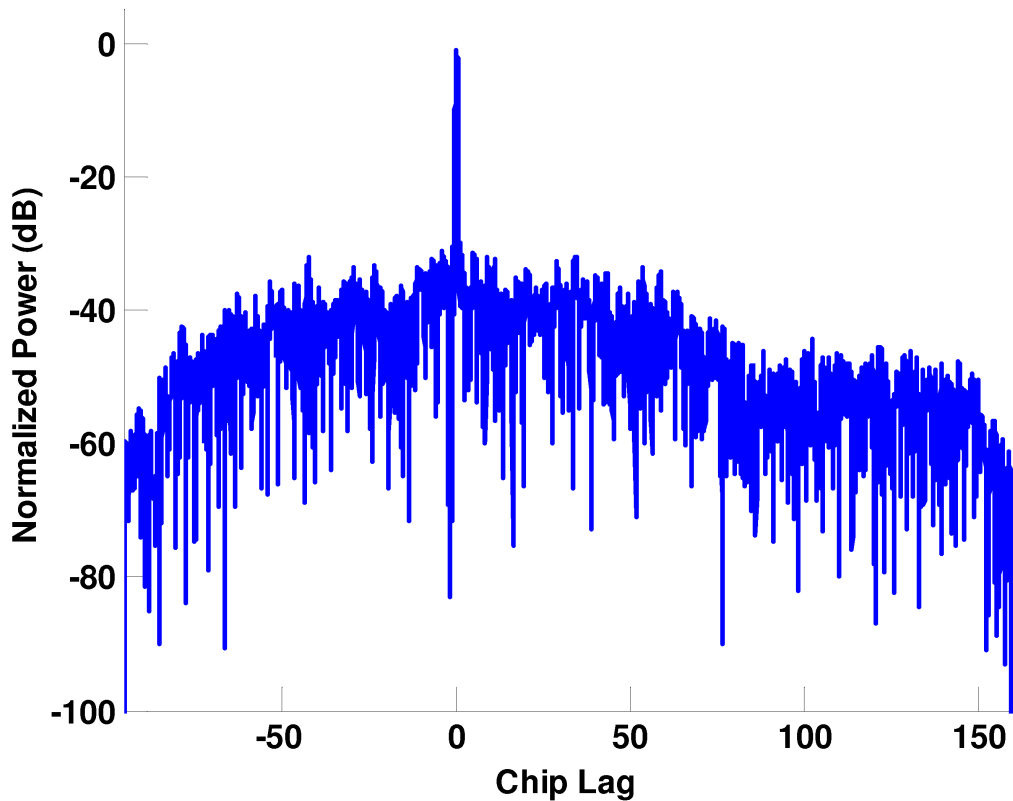


**Figure 4.5.** CPM Receiver Mismatch Filter Output Using length-64 Nunn-Kretschmer code with  $K = 10$  and Spoiled Resolution

and the mainlobe increased in width. The new PSL is approximately -29.8 dB

at a lag of about  $\pm 1.1$  as before. The normalized peak power (*i.e.* negative of mismatch loss) is approximately -1.1 dB.

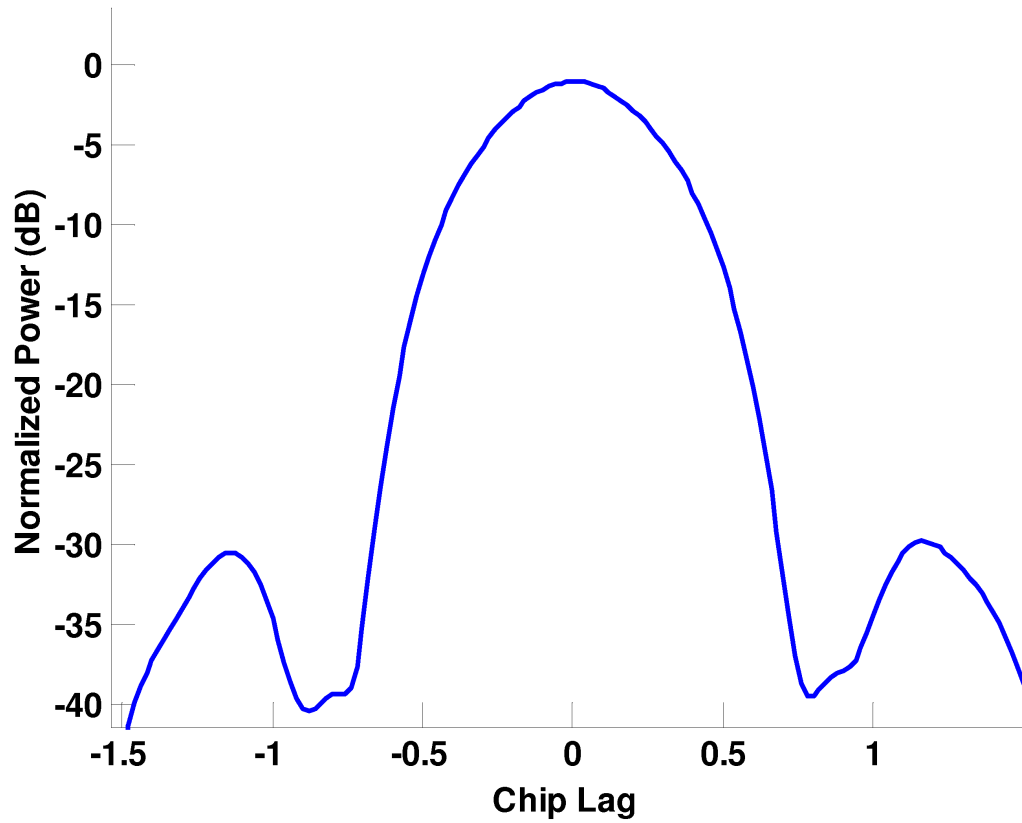


**Figure 4.6.** CPM Receiver Mismatch Filter Output Using length-64 Nunn-Kretschmer code with  $K = 10$  and Spoiled Resolution

## Chapter 5

# Waveform/Filter Evaluation

The characteristics of what is to be determined a “good” radar waveform must be defined. The foremost factor considered in this research is improvement in spectral efficiency. One particular set of parameters for spectral efficiency has been defined in [10]. This particular set of parameters is defined to refer to a type of waveform referred to as “spectrally clean”. While this particular set of parameters may not be a realistic metric in every situation presented here, it will still serve as a good goal to begin with. Another factor that must be satisfied for the waveform to be a reasonable choice is the suppression of range sidelobes. The choice of a phase modulated waveform leads to pulse compression and the compressed pulse must have sufficiently small range sidelobes to achieve a large dynamic range. A decent goal to start with for the peak sidelobe level (PSL) is -30 dB.

A selection of codes are evaluated in the following sections to give the CPM framework an adequate sampling of different code varieties. Codes taken into account here are a selection of Barker codes, MPS codes, polyphase Barker codes, the family of p-codes representing sampled LFM, and the family of Nunn-Kretschmer

codes optimized for mismatch filtering. The receiver filtering output will be characterized for waveforms generated from these codes for the matched and LS-based mismatch filtering treatments. Each waveform will be amplitude windowed with a Tukey window, using a full chip interval  $\tau$  for both the transition on and off, but the filter samples will be taken from an on/off version of the waveforms.

Spectral considerations can be compared to the NTIA guidelines discussed in Chapter 1. For the treatment considered here, waveforms will be quantified in spectral efficiency by determining the bandwidth required for some multiple of the chip frequency at a given suppression level.

## 5.1 Receive Matched Filter Results

Using the filter definition in Section 4.1 a selection of codes were modulated then paired with a filter for evaluation. The comb filter structure was employed with 5 samples per chip interval taken from the waveform in obtaining the filter. The over-sampling factor of 5 for these matched filter cases accounts for the continuous structure of the phase transitions in the CPM waveform. The analysis begins with the consideration of the largest three Barker codes.

### 5.1.1 Barker Waveforms

The Barker-coded waveforms are chosen for evaluation to set a baseline of performance in the CPM framework. Binary codes are commonly used and the Barker family is certainly the most famous. However, these codes are of insufficient length to be considered practical for use in pulse compression radars. Results of the receiver matched filter for the three longest Barker codes are shown in Figure 5.1. The peak sidelobes of the length-7 Barker-coded waveform are closer to the

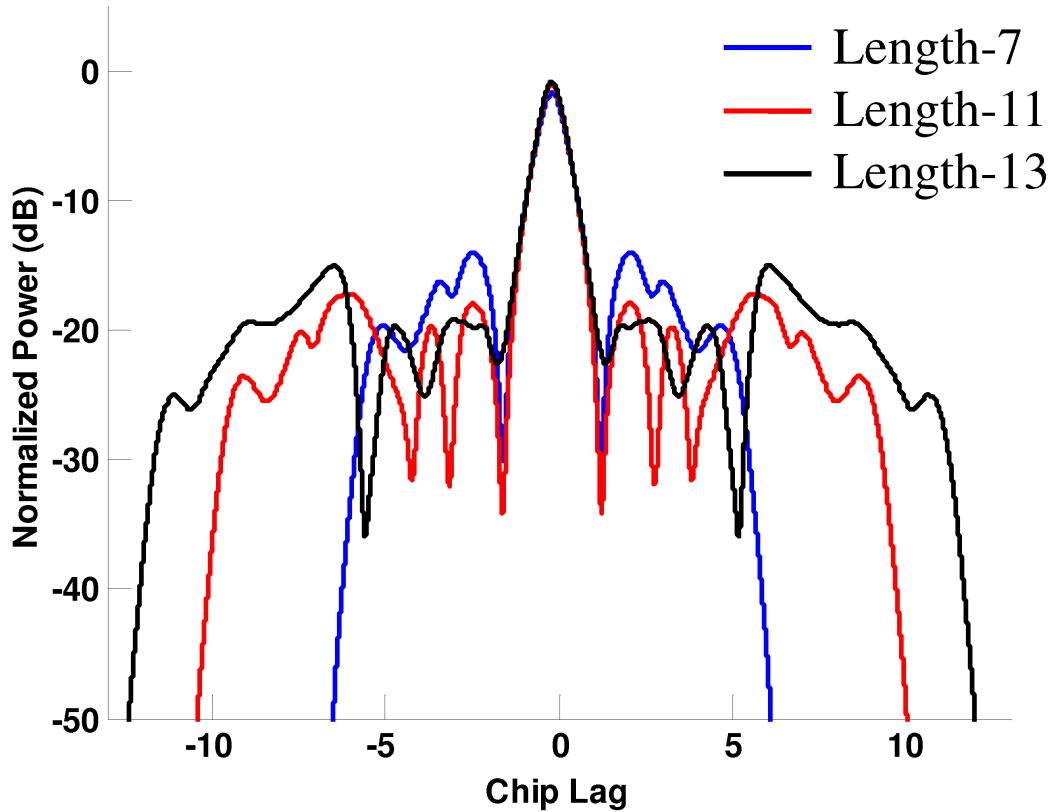


**Figure 5.1.** Receiver Matched Filter Results for Family of Barker-Coded CPM Waveforms

peak than the comparable peak sidelobes of the length-13 waveform. The length-11 waveform offers slightly better performance with regard to peak sidelobe level (PSL), with 2.2 dB lower PSL. The width of the mainlobe at the -3 dB level is less than one chip width for all three waveforms. The mainlobe width at -3 dB down from the peak is chosen to keep a consistent point of comparison with each waveform. The integrated sidelobe level (ISL) appears to be similar for each case, except that the concentration is at different locations relative to the peak.

Note there is a slight loss in the pulse compression gain for each of the three waveforms. This will be true for all matched filter cases. The reason for this

loss is due to the amplitude tapering of the transmitted waveform. From each chip interval, 5 evenly spaced samples are taken to form the matched filter for a given waveform. At the matched point, each sample will add maximum value with the exception of the tapered values at the beginning and end of the sampled waveform. For codes of shorter lengths, this loss will be more prominent. This result is important because the rise-/fall-time of the waveform must be considered to approximate a physically realizable pulse, and will also be a component of the loss in the receiver mismatch filtering results in Section 5.2.

A summary of results for Barker-coded waveforms based on Barker codes of length 7, 11 and 13 are presented in Table 5.1. The value of the ISL is found by

**Table 5.1.** Receiver Matched Filter Results From Select Barker-Coded CPM Waveforms

Code Length	Mainlobe Width	Peak Loss (dB)	PSL (dB)	ISL (dB)
7	$0.94\tau$	-1.71	-14.0	-5.8
11	$0.98\tau$	-1.05	-17.2	-6.6
13	$0.99\tau$	-0.88	-15.0	-4.9

taking the ratio of the power of the receiver filter output at all lags outside of 1 chip to the power within 1 chip. This value is presented in dB as a means of comparing the amount of sidelobe power contributed in each range interval with respect to the mainlobe. However, interpretation of the ISL results should be done with caution due to their relative nature (*e.g.* comparing codes of different lengths).

### 5.1.2 Polyphase Barker Waveforms

Results of the receiver matched filter outputs from the polyphase Barker-coded waveforms is shown in Figure 5.2. The worst of this selection of polyphase coded

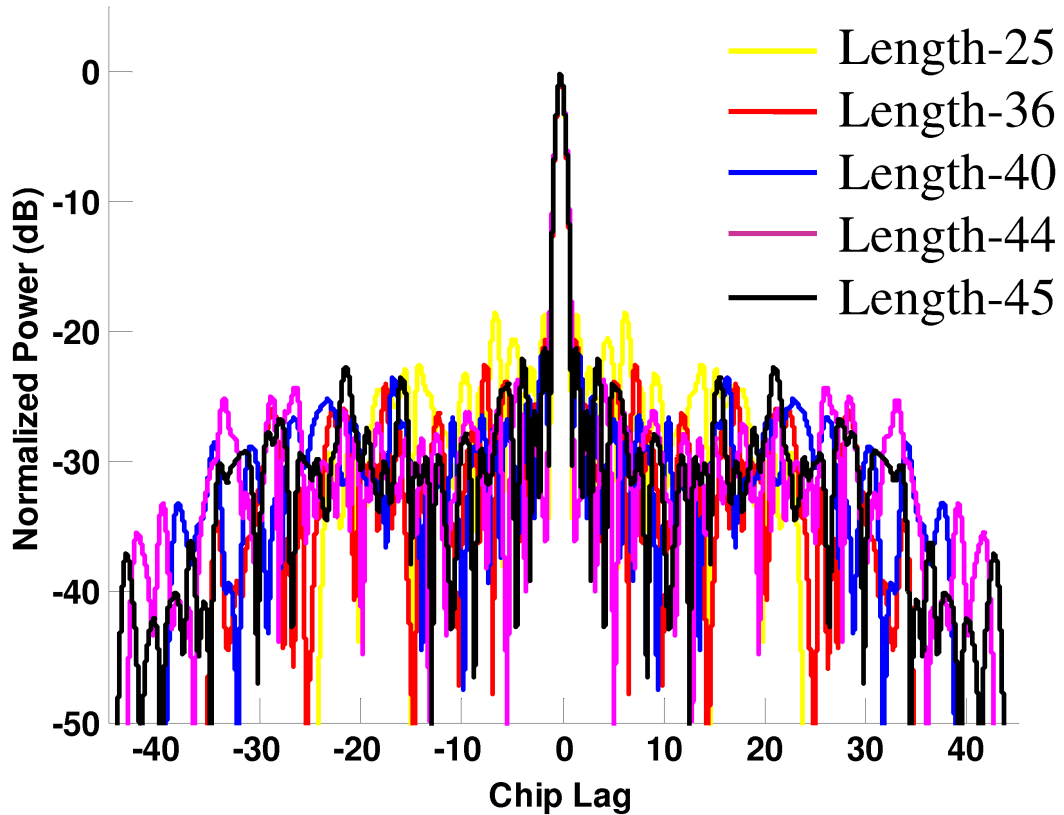


**Figure 5.2.** Receiver Matched Filter Results for Family of Polyphase Barker-Coded CPM Waveforms

waveforms is shortest, which is of length-25. The PSL for this waveform is approximately -18.5 dB. Again, the ISL is similar for all waveforms and the loss in the receiver filtering output decreases with code length as expected. The width of the mainlobe at the -3 dB point has some slight variation, but can be considered relatively constant. A summary of these results are given in Table 5.2. The best of these 5 codes is the length-44 polyphase Barker code. It offers a PSL of -23.7 dB at and a -3 dB mainlobe width of 1.22 times the chip interval. This PSL is 2.4 dB better than the length-45 polyphase Barker code. The narrowest mainlobes come from the shortest two codes, although these also have the largest sidelobes

**Table 5.2.** Receiver Matched Filter Results From Select Polyphase Barker-Coded CPM Waveforms

Code Length	Mainlobe Width	Peak Loss (dB)	PSL (dB)	ISL (dB)
25	$1.16\tau$	-0.45	-18.5	-7.2
36	$1.16\tau$	-0.31	-20.6	-9.7
40	$1.20\tau$	-0.28	-21.7	-9.3
44	$1.22\tau$	-0.25	-23.7	-9.5
45	$1.18\tau$	-0.24	-21.3	-9.0

by a factor of at least 3 dB relative to the length-44 code.

### 5.1.3 Minimum Peak Sidelobe Waveforms

Now another family of binary codes are considered. These are the Minimum peak sidelobe (MPS) codes. MPS codes offer benefits similar to the Barker codes. Longer code lengths are achieved by relaxation of the  $\frac{1}{M}$  PSL constraint. Figure 5.3 shows the receiver matched filter output for four codes ranging in length from 64 chips to 69 chips. A first look at the length-69 MPS code in black suggests that it outperforms the other three. It has a PSL of -19.1 dB. All of the mainlobes are vary close to 1 chip interval ( $\tau$ ) in time width. The length-69 code also offers the best ISL, 1.2 dB better than the length-64 MPS-coded waveform.

Table 5.3 summarizes the characteristics of the MPS-coded CPM waveforms. All mainlobe widths are within a tenth of a chip interval and the peak loss is

**Table 5.3.** Receiver Matched Filter Results From Select MPS-Coded CPM Waveforms

Code Length	Mainlobe Width	Peak Loss (dB)	PSL (dB)	ISL (dB)
64	$1.06\tau$	-0.17	-17.3	-3.5
67	$0.99\tau$	-0.16	-18.1	-3.4
68	$0.98\tau$	-0.16	-17.8	-3.7
69	$1.05\tau$	-0.16	-19.1	-4.7

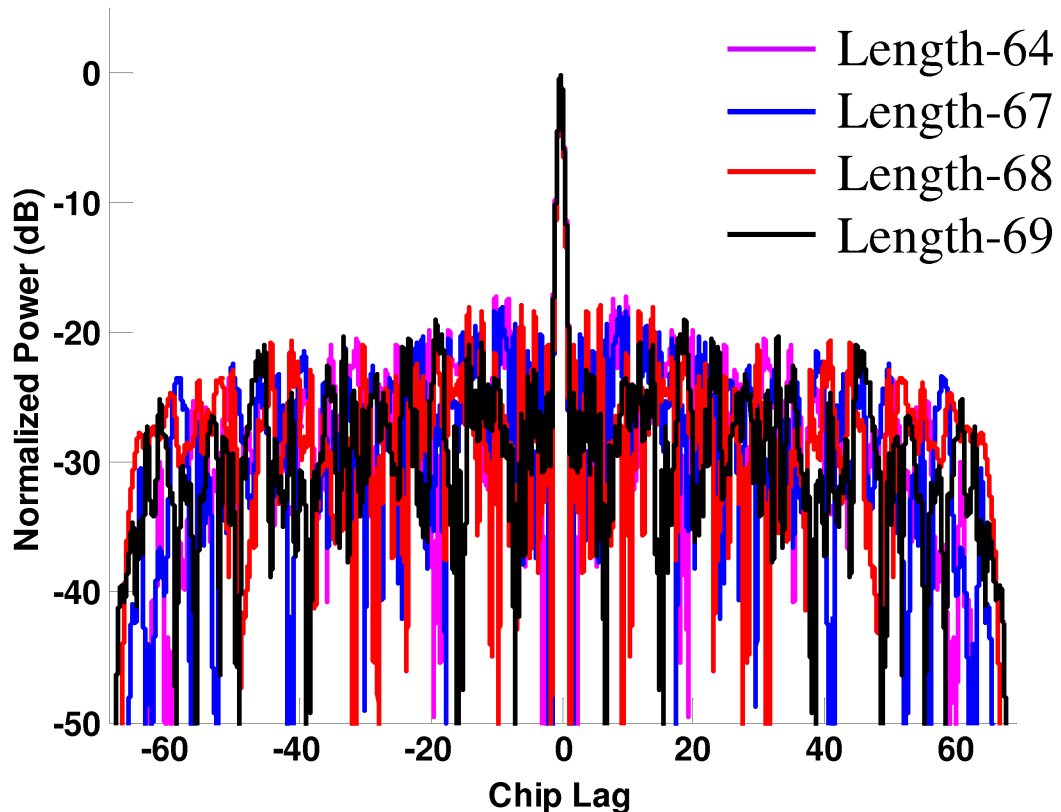


**Figure 5.3.** Receiver Matched Filter Results for Family of MPS-Coded CPM Waveforms

beginning to level out. The length-69 code outperforms the length-64 code by 1.8 dB in PSL. The results here are noticeably higher than those presented for the polyphase Barker codes in Table 5.2. The difference in PSL between the length-44 polyphase Barker code and the length-69 MPS code is 4.5 dB. This further solidifies the benefit in having the ability to implement polyphase codes. The CPM framework naturally applies itself to any general phase code, which is a tremendous benefit.

#### 5.1.4 P-code Waveforms

P-codes are based on linear frequency modulation (LFM). Results of the P-code based CPM waveforms work better with the square chip shaping filter described in (2.9), due to the linear nature in the frequency change. However, in order to keep a constant base for comparison, the raised cosine filter in (3.4) is kept as the chip shaping filter for the CPM framework. The length of the P-code is an input parameter. All have been chosen to be 64 chips in length to make similar comparisons to other codes with similar chip counts. The P-3 code has

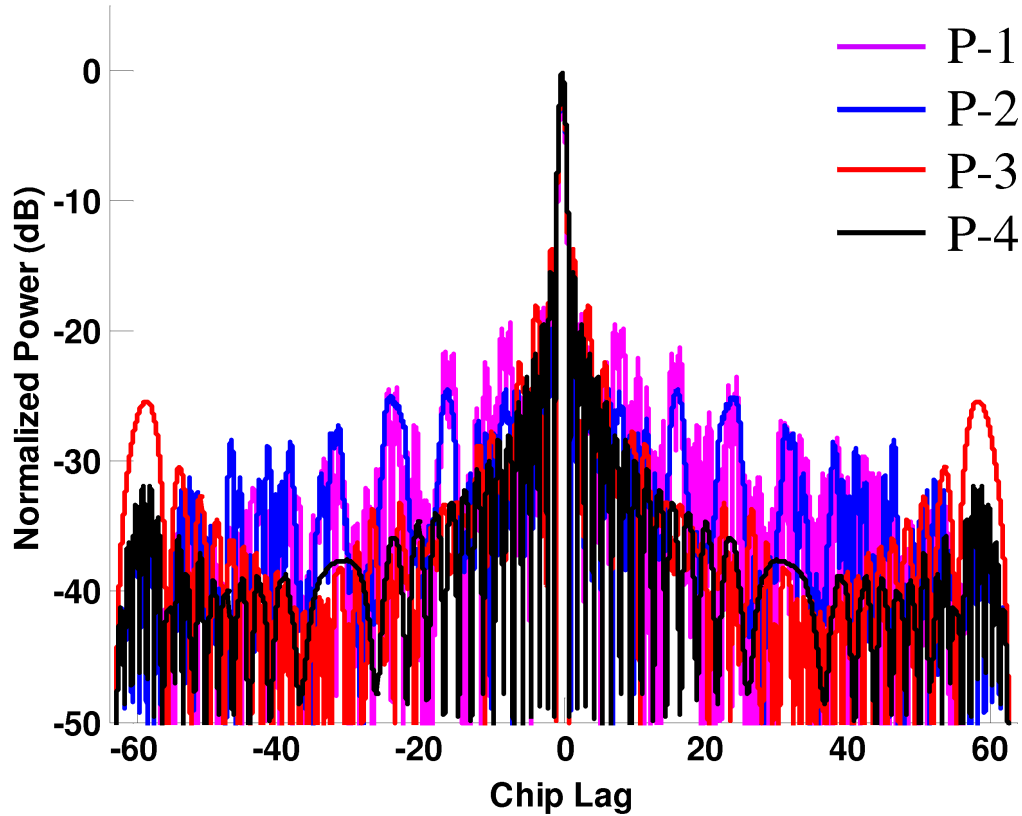


**Figure 5.4.** Receiver Matched Filter Results for Family of P-Code CPM Waveforms

large outer lobes in the correlation output. The P-2 code has the best PSL at

-19.9 dB. The worst PSL is 6.1 dB greater and is the P-3 code. The P-4 code has the best ISL which is -9.9 dB. This is the lowest ISL for the receiver matched filter outputs. All mainlobe widths at the -3 dB level are slightly larger than a chip interval. The P-4 code has the widest mainlobe of  $1.21\tau$ . Table 5.4 summarizes the characteristics of the P-code based CPM waveforms.

**Table 5.4.** Receiver Matched Filter Results From Select P-Code CPM Waveforms

Code (length-64)	Mainlobe Width	Peak Loss (dB)	PSL (dB)	ISL (dB)
P-1	$1.03\tau$	-0.17	-15.9	-6.7
P-2	$1.14\tau$	-0.17	-19.9	-8.6
P-3	$1.15\tau$	-0.17	-13.8	-7.6
P-4	$1.21\tau$	-0.17	-15.5	-9.9

### 5.1.5 Nunn-Kretschmer Waveforms

The family of Nunn-Kretschmer phase codes were specifically optimized for LS-based mismatch filtering. However, analysis of the matched filtering can give an initial comparison to the other codes considered. Results of the receiver mismatch filter for the four codes presented in [15] are shown in Figure 5.5. Table 5.5 summarizes the characteristics of the Nunn-Kretschmer CPM waveform.

**Table 5.5.** Results From the Family of Nunn-Kretschmer CPM Waveforms

Code	Length	Mainlobe Width	Peak Loss (dB)	PSL (dB)	ISL (dB)
Nunn-1	32	$1.22\tau$	-0.35	-21.1	-7.9
Nunn-2	32	$1.22\tau$	-0.35	-20.5	-7.9
Nunn-3	32	$1.18\tau$	-0.35	-19.7	-7.5
Nunn-4	64	$1.22\tau$	-0.17	-21.4	-8.8

The first 3 codes have 32 chips and the fourth has 64 chips and is the code used in Section 3.2. The Nunn-4 code is listed in Table 3.1. The best PSL performance

comes from the longest of the 4 codes, but only by 0.3 dB. This is not very much considering the length of the Nunn-1 coded waveform is half that of the Nunn-4. The length-32 Nunn-3 coded waveform has the worst performance with regards to ISL, with a value of -7.5 dB. The best result in mainlobe width comes from the Nunn-3 code at a value of  $1.18\tau$ . However, this code also has the worst performance in PSL with a peak sidelobe of -19.7 dB relative to a peak output of 0 dB.

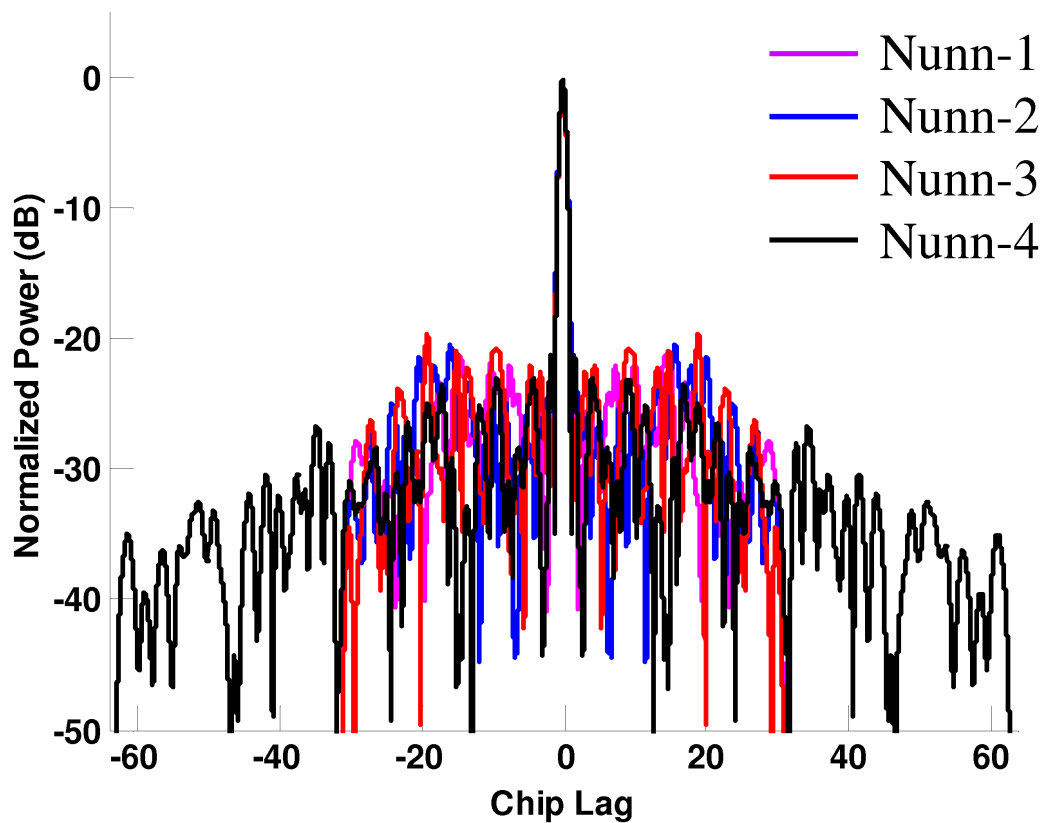


**Figure 5.5.** Receiver Matched Filter Results for Family of Nunn-Kretschmer CPM Waveforms

## 5.2 Receive Mismatch Filter Results

Using the filter definition in (4.8) from Section 4.2 the same codes used in Section 5.1 were modulated then paired with a mismatch filter for evaluation. The oversampled version of this filtering gives a super-resolution result which can then be exploited to further reduce the range sidelobes. This is evident in the PSLs and ISLs of the receive filtering outputs. For the filters calculated here an oversampling factor of  $K = 10$  is used. To return to the nominal resolution of the waveform the 10 rows surrounding the  $m^{th}$  row are removed (5 above and 5 below) from  $\mathbf{A}_{\text{CPM}}$  defined in (4.7).

### 5.2.1 Barker Waveforms

Revisiting the three Barker-coded waveforms using codes of lengths 7, 11 and 13 from Table 2.1, receiver mismatch filtering results are presenting in Figure 5.6 and Table 5.6. The general envelopes of the range sidelobes have been reduced considerably. And even though the range over which sidelobes are present due to the increased length of the receive filter are extended, the ISL for each Barker-coded waveform has decreased, by 2.5 dB for the length-7 code and by 2.6 for the length-13 code.

**Table 5.6.** Mismatch Filter Results From Select Barker-Coded CPM Waveforms

Code Length	Mainlobe Width	Peak Loss (dB)	PSL (dB)	ISL (dB)
7	$0.29\tau$	-4.13	-19.8	-8.3
11	$0.32\tau$	-3.28	-19.8	-7.0
13	$0.50\tau$	-1.68	-20.3	-7.5

The best performer for the matched filter was the length-11 code with a PSL of -17.2 dB. This has decreased by 2.6 dB for the receiver mismatch filter. The best

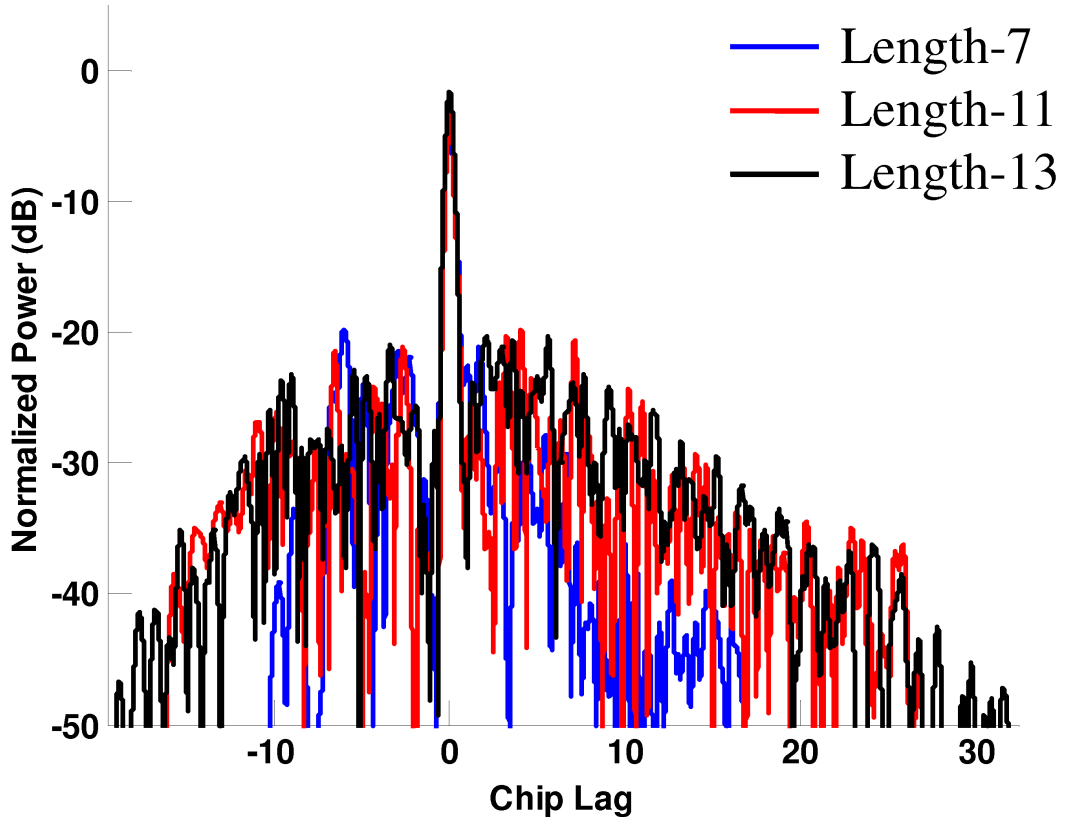


**Figure 5.6.** Receiver Mismatch Filter Results for Family of Barker-Coded CPM Waveforms

case in mismatch filtering is now the length-13 Barker-coded waveform with PSL of -20.3 dB, down 5.3 dB relative to the matched filter case for the same waveform. The mainlobe widths at the -3 dB point are considerably narrower. This is because the resolution spoiling technique applied to LS-matrix  $\mathbf{A}_{\text{CPM}}$  increases sidelobe levels further from the peak first, which is seen as a widening of the base. Sidelobes closer to the peak are increased as more spoiling is introduced in an outside-to-in fashion with respect to the peak. Thus the width of the mainlobe at the level of the peak sidelobe is comparable, but near the peak at the -3 dB point some super-resolution properties still exist. The pulse compression loss has also increased, but

this effect should diminish as longer code lengths are considered.

### 5.2.2 Polyphase Barker Waveforms

The polyphase Barker-coded waveforms presented in Section 5.1.2 show a descent increase in performance, especially for the longer code lengths. Results from the receiver mismatch filtering are shown in Figure 5.7. The code lengths of 44

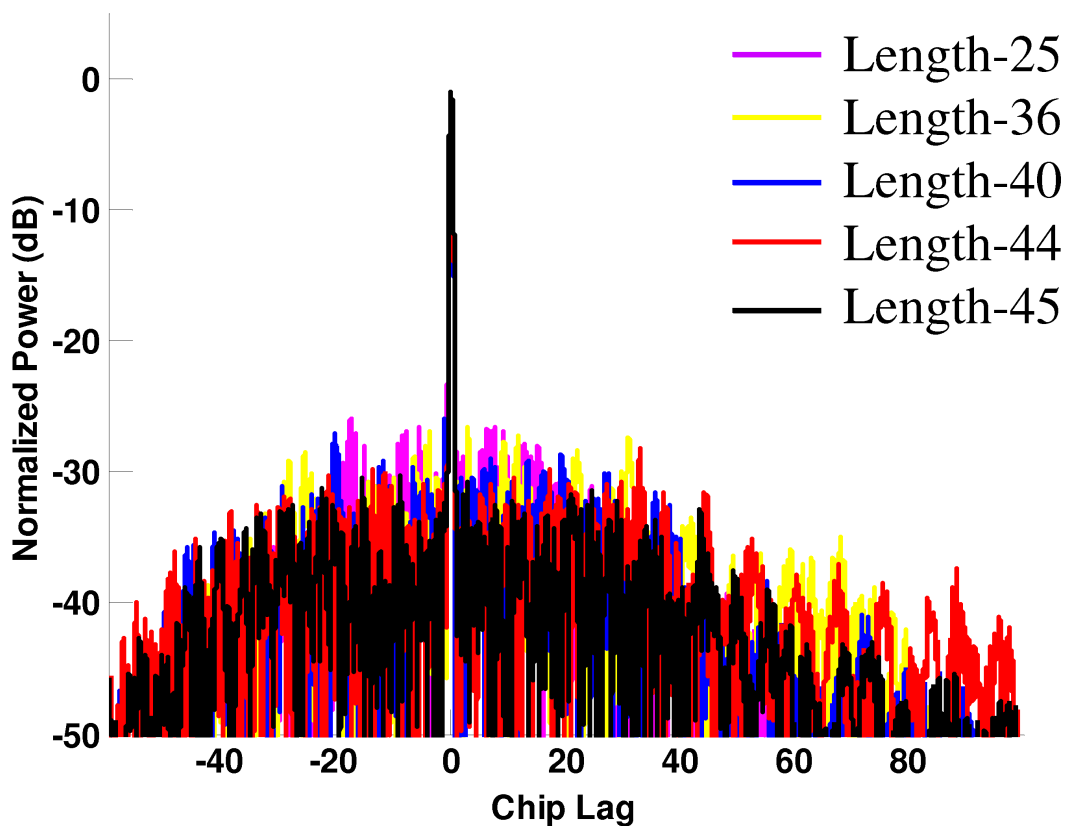


**Figure 5.7.** Receiver Mismatch Filtering Results for Polyphase Barker-Coded CPM Waveforms

and 45 show the best results, with PSLs near -30 dB and a narrow, isolated mainlobe. The waveforms of the shorter codes still have sidelobes around -25 dB closer to the peak. It is also evident that the mainlobe becomes narrower towards the peak, an indication that some of the super-resolution effects are still in play.

Comparing the receiver filter results from the matched and mismatch cases of polyphase Barker-coded waveforms in Tables 5.2 and 5.7 show improvement in all categories. Mainlobe widths are relatively close to one half of a chip interval for

**Table 5.7.** Mismatch Filter Results For Polyphase Barker-Coded CPM Waveforms

Code Length	Mainlobe Width	Peak Loss (dB)	PSL (dB)	ISL (dB)
25	$0.54\tau$	-2.31	-25.9	-10.3
36	$0.53\tau$	-1.99	-26.7	-10.3
40	$0.55\tau$	-1.05	-26.0	-11.5
44	$0.52\tau$	-1.56	-28.2	-11.2
45	$0.65\tau$	-0.99	-30.2	-13.9

all five waveforms at the -3 dB level in the mismatch filtering. This is double the resolution seen in the receiver matched filter case for the same waveform. The ISL has decreased by a decent amount, with a 3.1 dB improvement for the length-25 code and a 4.9 dB improvement for the length-45 code. The PSL has improved by as much as 9 dB. The best performer is now the length-45 polyphase Barker code with a PSL of -30.2 dB, which is a suitable result. Losses in mainlobe power, hence lower SNR, have increased but the effect is certainly less than what was seen in the shorter binary Barker codes.

### 5.2.3 Minimum Peak Sidelobe Waveforms

The LS-based mismatch filtering for the MPS codes begins to show improvement towards the -30 dB PSL goal for all three codes. In Figure 5.8 the length-64 MPS-coded waveform is the worst with a PSL of -27.8 dB. However, this is an improvement of 10.5 dB from the matched filter case. Further, the width of the mainlobe at the -3 dB point is a quarter of the width for the matched filter. This indicates that the sidelobes could be reduced further by removing more rows from

the LS-matrix  $\mathbf{A}_{\text{CPM}}$ , though the base of the mainlobe will widen as well. There

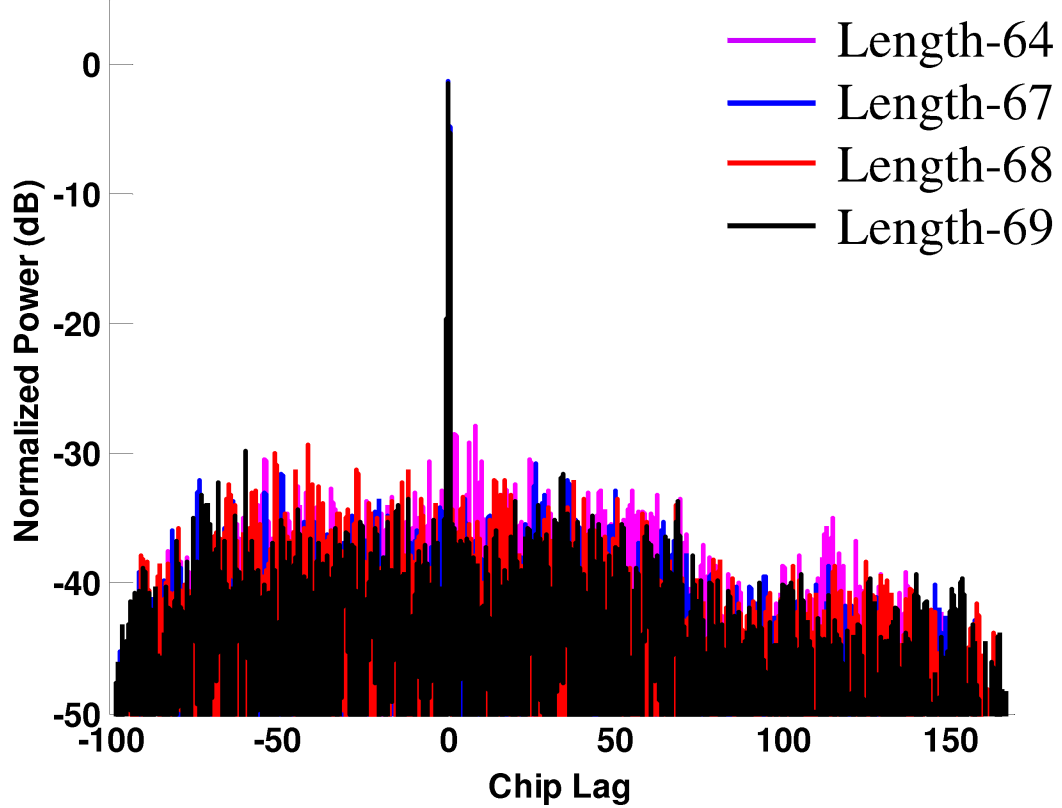


**Figure 5.8.** Receiver Mismatch Filter Results for Family of MPS-Coded CPM Waveforms

is a problem with the increase width as the base of the mainlobe. The width at the base tends to increase at a faster rate than the top. A trade-off is presented to continue removing rows from  $\mathbf{A}_{\text{CPM}}$  until the width at the PSL is “spoiled” to a specified design point. Results from Figure 5.8 are tabulated and presented in Table 5.8. Some particular notes of the MPS receiver mismatch filter results include the trend of a decrease in ISL. The ISL of the length-64 MPS coded waveform has decreased by 4.9 dB. The best improvement of ISL is for the length-69 code with a decrease of 7.3 dB. The best code, the length-67 MPS code, offers the best PSL

**Table 5.8.** Mismatch Filter Results From Select MPS-Coded CPM Waveforms

Code Length	Mainlobe Width	Peak Loss (dB)	PSL (dB)	ISL (dB)
64	$0.26\tau$	-2.46	-27.8	-8.4
67	$0.36\tau$	-1.33	-30.8	-11.9
68	$0.28\tau$	-2.03	-29.3	-9.9
69	$0.35\tau$	-1.57	-29.7	-12.0

of the four different lengths at a value of -30.8 dB, an decrease of 12.7 dB from the matched filter output. This code also has the smallest mismatch loss in the peak at -1.33 dB. Recall that there is a small loss associated with the rise-/fall-time of the waveform amplitude. This value was -0.16 dB for the matched filter case.

#### 5.2.4 P-code Waveforms

The LFM-based waveforms are not particularly suited for the CPM framework. The receiver mismatch filter has narrow sidelobes cascading down on the sides of the mainlobe. This can be seen in the inset of Figure 5.9 as a wider base around -25 dB. The P-1 code has the largest peak sidelobe of -17.7 dB at a lag of 32 chips away from the mainlobe. The best code appears to be the P-2 coded waveform in blue with an approximate -26.9 dB normalized sidelobe magnitude around a chip lag of -8.5 chips.

Table 5.9 summarizes the characteristics of the P-code based CPM waveform receiver mismatch filtering. Note that even though the width of the mainlobe is narrow at the -3 dB point, it has spread near the base, as described above. The results of the P-2 code are good in all categories, the mainlobe width and peak loss are the second best of the four by a narrow margin. The PSL and ISL are very good at -26.9 dB and -13.8 dB respectively. The ISL of -13.8 dB is the best seen so far with the exception of the very short Barker codes. The second best

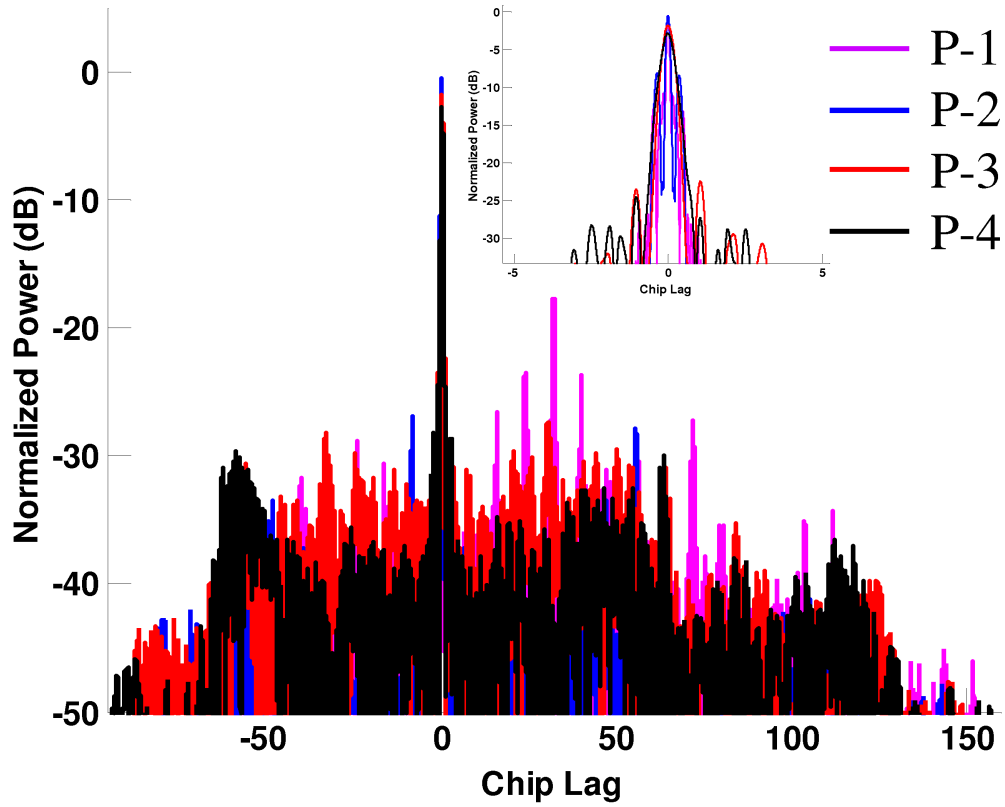


**Figure 5.9.** Receiver Mismatch Filter Results for Family of P-Code CPM Waveforms

**Table 5.9.** Receiver Mismatch Filter Results From Select P-Code CPM Waveforms

Code (length-64)	Mainlobe Width	Peak Loss (dB)	PSL (dB)	ISL (dB)
P-1	$0.12\tau$	-0.52	-17.7	-9.1
P-2	$0.17\tau$	-0.58	-26.9	-13.8
P-3	$0.42\tau$	-1.84	-22.4	-8.7
P-4	$0.42\tau$	-2.87	-24.4	-10.5

PSL is -24.4 dB from the P-4 code, but it also has the worst peak loss of -2.87 dB.

### 5.2.5 Nunn-Kretschmer Waveforms

The Nunn-Kretschmer coded waveforms have the best possibility for being good performers in LS-based mismatch filters, because that is the framework in which they were optimized. However, the optimization was based on the “ideal” waveform. Figure 5.10 shows the results for receiver mismatch filtering of the Nunn-Kretschmer coded CPM waveforms. Here a nice narrow peak is seen with

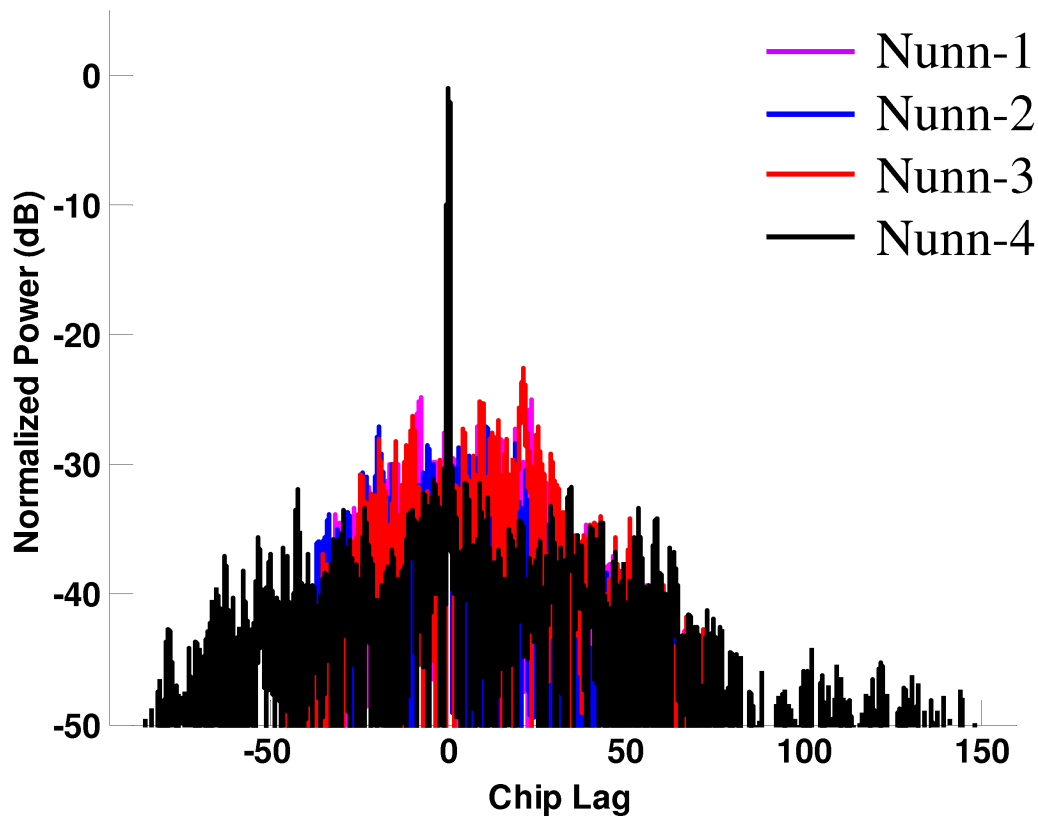


**Figure 5.10.** Receiver Mismatch Filter Results for Family of Nunn-Kretschmer CPM Waveforms

what appears to be very low ISLs. The Nunn-4 code in black is the longest with

64 chips, and appears to be the best. The other 3 codes have 32 chips each, and all have PSLs below -20 dB.

Table 5.10 summarizes the characteristics of the Nunn-Kretschmer CPM waveform. The best PSL does come from the longer Nunn-4 code. The ISL for all the

**Table 5.10.** Results From the Family of Nunn-Kretschmer CPM Waveforms

Code	Length	Mainlobe Width	Peak Loss (dB)	PSL (dB)	ISL (dB)
Nunn-1	32	$0.59\tau$	-1.31	-24.9	-11.1
Nunn-2	32	$0.61\tau$	-1.79	-27.1	-12.1
Nunn-3	32	$0.63\tau$	-1.27	-22.5	-9.7
Nunn-4	64	$0.67\tau$	-1.09	-30.2	-14.2

Nunn-Kretschmer codes have improved. The average level of the sidelobes in the band of  $\pm 50$  chips around the peak is fairly constant. The best ISL value is -14.2 dB for the Nunn-4 code and the worst is -9.7 dB from the Nunn-3 code. The -3 dB widths of the mainlobe for all 4 codes are nearly the same at approximately 0.6 times the width of a chip. The Nunn-Kretschmer codes are all good performers and a strong proponent for the use of optimized codes.

### 5.3 Spectral Analysis

To analyze the spectral properties of the CPM waveforms, power spectral densities (PSDs) are simulated. The code with the best PSL from receiver *mismatch* filtering is chosen from the MPS, polyphase Barker, P-, and Nunn-Kretschmer codes. Codes of the same family have near similar results for their respective PSDs, so one code per family is sufficient to characterize the waveform. The Barker code is excluded due to its short length and limited PSL performance in receiver filtering. The power level is normalized to the maximum power, and the

frequency is normalized to the frequency of the chips, or chip rate. Recall that the waveforms were modulated using the CPM radar model with the raised cosine filter defined in (3.4). Also, severe oversampling is performed in order to produce a near continuous waveform. The results found here use a sampling rate of 500 samples per chip for the PSD calculation.

The codes chosen for simulation are the length-67 MPS code, the length-45 polyphase Barker code, the length-64 P-2 code and the length-64 Nunn-4 code. The results are plotted in Figure 5.11. All of the four codes have a two-sided

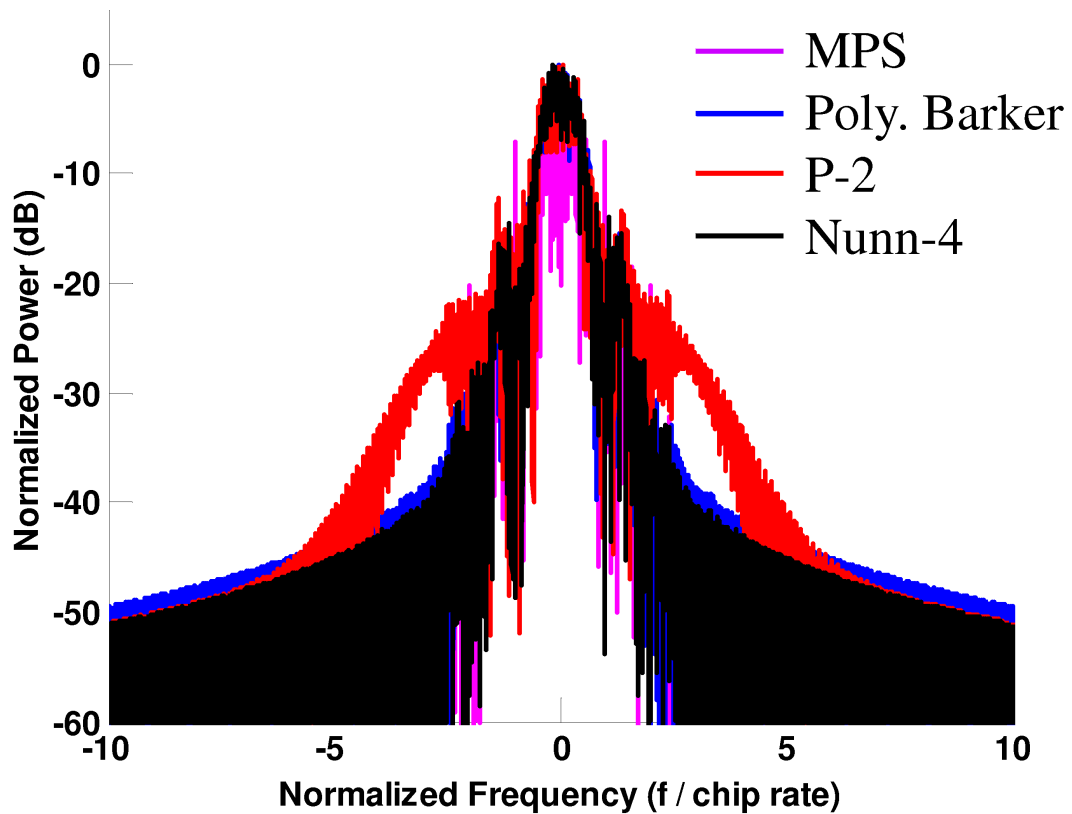


**Figure 5.11.** PSD Results for the Best PSL Performer of MPS, Polyphase Barker, P-Code, and Nunn-Kretschmer Codes

bandwidth of approximately 3 times the chip rate at a level of -20 dB down from

the peak. All codes have a PSD down around -50 dB relative to the peak at the baseband frequencies of  $\pm 10$  times the chip frequency. Note that the large spikes are still present in the binary-coded waveform.

The codes all have a similar envelope of their PSD, except for the P-code for the frequencies of about  $\pm 2 - \pm 6$  times the chip rate. It is expected that there is a mismatch with the linear nature of the phase changes in the P-code and the non-linear property of the raised cosine chip shaping filter. To determine if this is the case, the rectangular filter from (2.9) is used for the CPM waveforms used to calculate the PSDs in Figure 5.11. The large lobes of the P-2 code have reduced,

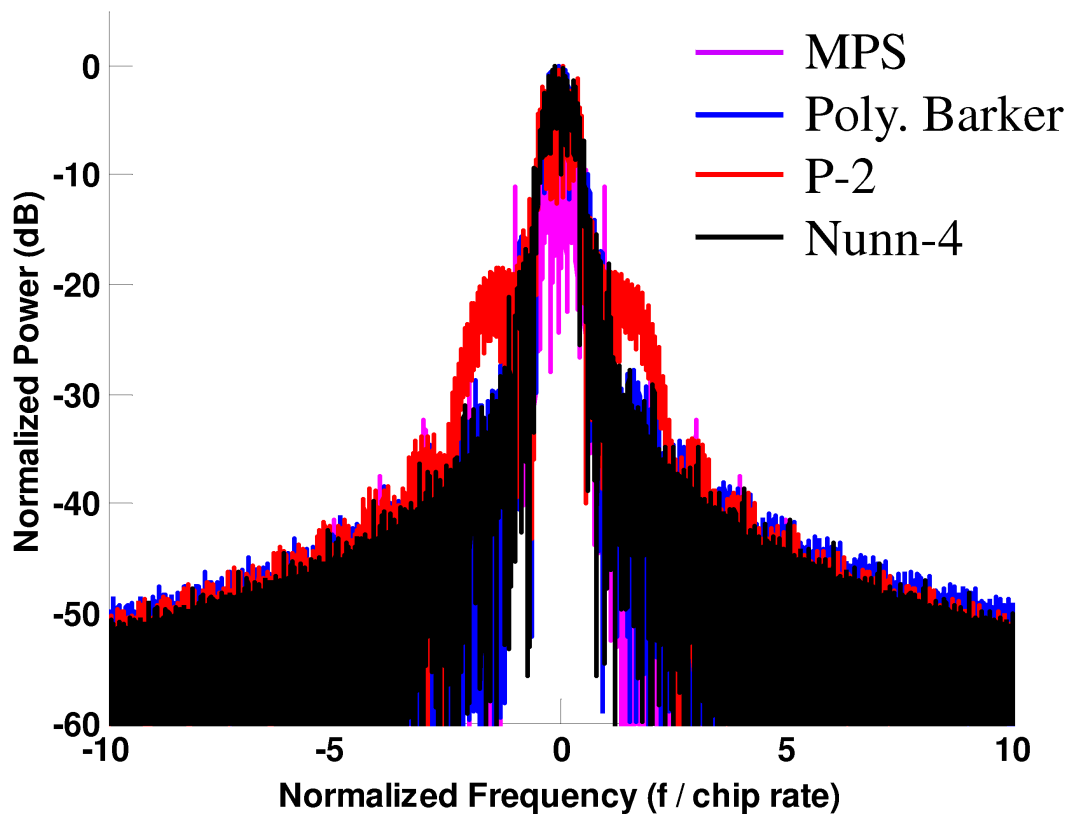


**Figure 5.12.** PSD Results for the Best PSL Performer of MPS, Polyphase Barker, P-Code, and Nunn-Kretschmer Codes with Rectangular Chip Shaping Filter

but are still prominent relative to the other waveforms. With this result and the knowledge of the spikes present in the binary codes, polyphase codes with pseudo-random phase transitions seem best suited for a confined PSD.

As one final analysis of the PSD of the CPM encoded waveform, a window will be applied to the waveforms based on the four codes listed above. A Tukey window is chosen with an on/off transition time lasting the duration of the first and last chips respectively. The PSD results for these waveforms is shown in Figure 5.13. The raised cosine chip shaping filter was used again in the CPM setup for consistency with previous tests. The results shown here indicate an

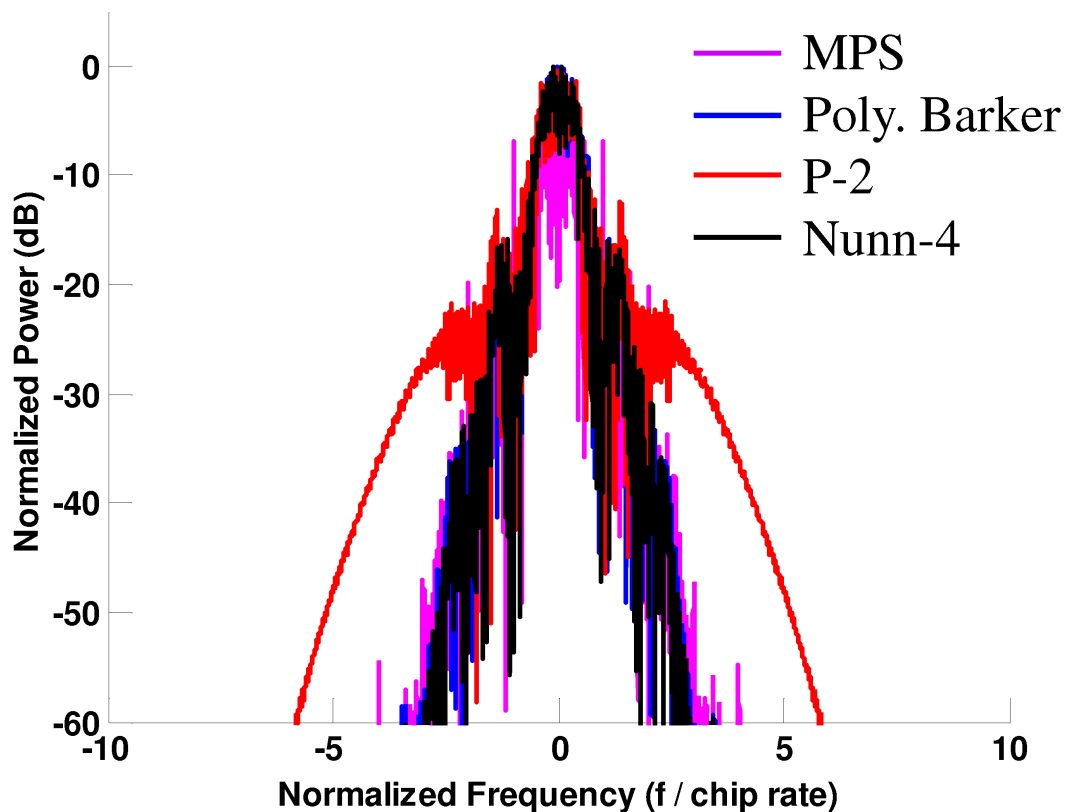


**Figure 5.13.** PSD Results for the Best PSL Performer of MPS, Polyphase Barker, P-Code, and Nunn-Kretschmer Codes with Tukey Amplitude Window

extremely band-limited waveform, with very sharp spectral drop-off. Even the odd-shaped envelope of the P-2 coded waveform is at -60 dB at frequencies of  $\pm 6$  times the chip rate. The other three waveforms are at the -60 dB level by  $\pm 4$  times the chip frequency.

## 5.4 Experimental Results

A radar testbed was used to obtain results for a CPM waveform. The results from the spectrum analyzer are shown in Figure 5.14. The length-64 Nunn code

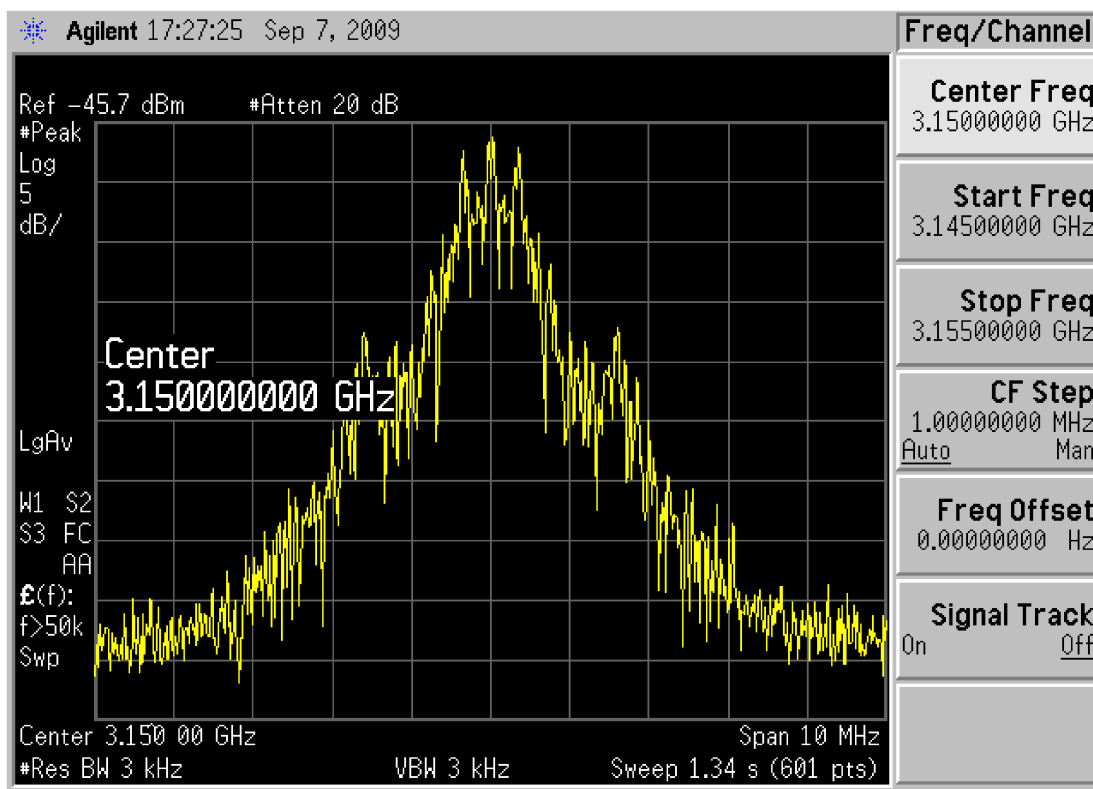


**Figure 5.14.** Spectrum Analyzer Results for CPM Waveform

was used to modulate a CPM waveform under the framework presented in Section 3.1 at a sample rate of 1 gigasample per second (Gsps). The chip duration is

$\tau = 200$  nanoseconds for a total pulse width of 12.8 microseconds. A duty cycle of 25% was chosen for a pulse repetition interval (PRI) of 51.2 microseconds. The waveform was not passed through a power amplifier for these results.

To determine if any spectral regrowth effects are introduced by the waveform, a second experiment was conducted and the PSD of the waveform was measured after it was amplified through a power amplifier. These results are displayed in Figure 5.15. Comparing the results in Figure 5.14 to Figure 5.15 it is seen that

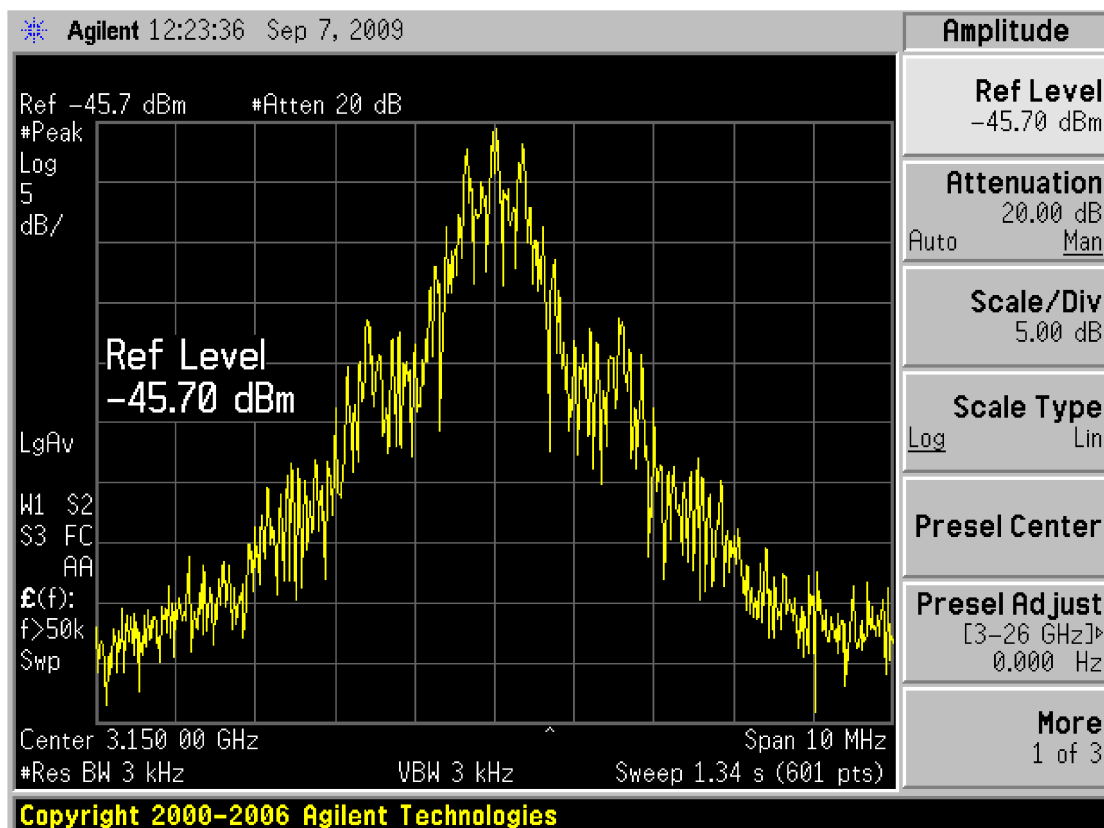


**Figure 5.15.** Spectrum Analyzer Results for CPM Waveform

the two power spectral densities are nearly identical. This is evidence that the Nunn-coded CPM waveform did not introduce any spectral regrowth after passing through the amplifier.

# Chapter 6

## Conclusion

The Continuous Phase Modulation (CPM) framework, well-known in the aeronautical telemetry community as a means to achieve both high spectral efficiency and high power efficiency, has been applied to the implementation of radar waveforms. The communications based model was first considered, but it was shown that it was inadequate to modulate a radar waveform with acceptable levels of range sidelobes. A new framework, more suited for radar waveform design, was created so that the CPM waveform mimics the “ideal” waveform as closely as possible without spoiling the power and spectral efficiency benefits gained from CPM. Because radar codes are generally determined within an implicit infinite bandwidth framework, application of CPM has been found to still induce some degradation in terms the peak sidelobe level (PSL) in the receiver matched filter output. However, this problem has been addressed with an alternate signal processing technique in the receiver.

A version of the Least Squares (LS) based mismatch filter was employed as a technique to reverse some of the degradation effects induced by CPM. The original LS-based mismatch filter is implicitly based on the “ideal” pulse compression

waveform. The result of the CPM waveform deviation from the Ideal is that the nominal mismatch filter will not work sufficiently when applied to the received CPM waveform. However, using the mismatch filter formulation with an over-sampled version of the CPM waveform does result in a waveform/filter pair that achieves good spectral containment, is power efficient, and provides low range sidelobes. This framework initially produces a super-resolution result, but with a resolution spoiling technique, sidelobe levels can be further suppressed while returning to nominal resolution.

All waveforms considered are constant modulus, hence power efficient. The beginning and end of the waveform still needed to be addressed, though, in order to further reduce the spectral spreading by eliminating the rapid amplitude transition during the pulse rise-time and fall-time. This was addressed by two models with similar results. The first model considered linear rise-time transition over a single chip interval  $\tau$ , and the same for fall-time transition. The second model considered used a Tukey window to transition over the same portions of the waveform. Both models showed that the spectral envelope of the CPM waveform can be very well contained with this amplitude tapering.

A collection of code families were considered for the receiver matched and mismatch filter applications. These codes were the Barker code, polyphase Barker code, minimum peak sidelobe (MPS) code, P-codes, and four Nunn-Kretschmer codes. Mismatch filtering was shown to be superior to matched filtering in terms of peak sidelobe level with minimal loss in pulse compression gain. With the exception of the limited length Barker codes and the most of the P-codes, all code families produced acceptable peak sidelobe levels and a relative improvement in integrated sidelobe level.

## Future Work

There are many avenues that can be followed with the results of this research. Initially, one could ask if it is possible to design an optimal code based on the CPM framework. The codes used for this research were previously designed with the “ideal” implementation in mind, without regard for the degradation of the actual physical waveform that is induced in the transmitter. However, if the continuous nature of the CPM waveform is taken into account, perhaps a code designed to accommodate the CPM structure could produce even better results.

Another avenue to consider is the implementation of the amplitude taper in an actual radar system power amplifier. The power efficient amplifiers currently used are non-linear in the transition region and effects on the spectral spreading and range sidelobes need further investigation. Initial results imply that some non-linearities, such as a squared cosine rise-/fall-time, have little effect on the spectral containment, but further analysis is necessary.

Finally, another consideration could be the embedding of information in the phase transition of the code. The phase codes, particularly the binary codes, can be transitioned in the positive or negative direction to get to the same phase value. This is effectively an increase or decrease in frequency shifts respectively. The CPM framework is immediately ready for such a consideration with a simple modification of the differential encoding described in (3.3). There are certainly other aspects that can be considered but these three seem to be most suitable for near term research.

# References

- [1] M. I. Skolnik, *Introduction to radar systems*. McGraw-Hill, 3 ed., 2001.
- [2] S. Kingsley and S. Quegan, *Understanding radar systems*. SciTech Publishing, Inc., 1999.
- [3] S. Blunt, M. Cook, E. Perrins, and J. de Graaf, “Cpm-based radar waveforms for efficiently bandlimiting a transmitted spectrum,” in *IEEE Radar Conference*, 4-8 May 2009.
- [4] N. Levanon and E. Mozeson, *Radar signals*. John Wiley & Sons, Inc., 2004.
- [5] R. L. Frank, “Polyphase codes with good nonperiodic correlation properties,” *IEEE Transactions on Information Theory*, vol. 9, pp. 43 – 45, 1963.
- [6] A. R. Brenner, “Polyphase barker sequences up to length 45 with small alphabets,” *Electronic Letters*, vol. 34, pp. 1576 – 1577, August 6 1998.
- [7] J. D. Jenshak and J. M. Stiles, “A fast method for designing optimal transmit codes for radar,” in *IEEE Radar Conference*, pp. 1 – 6, May 26 - 30 2008.
- [8] J. D. Jenshak and J. M. Stiles, “Transmit coding with a range ambiguity,” in *International Waveform Diversity and Design Conference*, pp. 98 – 102, February 8 - 13 2009.

- [9] C. J. Nunn and G. E. Coxson, "Polyphase pulse compression codes with optimal peak and integrated sidelobes," *IEEE Transactions on Aerospace and Electronic Systems*, vol. 45, pp. 775 – 781, April 2009.
- [10] H. H. Faust, B. Connolly, T. M. Firestone, R. C. Chen, B. H. Cantrell, and E. L. Mokole, "A spectrally clean transmitting system for solid-state phase-array radars," in *Radar Conference*, pp. 140–144, 26-29 April 2004.
- [11] J. B. Anderson, T. Aulin, and C.-E. Sundberg, *Digital Phase Modulation*. Plenum Press, 1986.
- [12] L. Lifang and M. K. Simon, "Performance of coded oqpsk and mil-std soqpsk with iterative decoding," *IEEE Transactions on Communications*, vol. 52, pp. 1890 – 1900, November 2004.
- [13] B. E. Rimoldi, "A decomposition approach to cpm," *IEEE Transactions on Information Theory*, vol. 34, pp. 260 – 270, March 1988.
- [14] E. Perrins and M. Rice, "Pam representation of ternary cpm," *IEEE Transactions on Communications*, vol. 56, pp. 2020 – 2024, December 2008.
- [15] C. Nunn and F. F. Kretschmer, "Performance of pulse compression code and filter pairs optimized for loss and integrated sidelobe level," in *IEEE Radar Conference*, pp. 110–115, 17-20 April 2007.
- [16] R. Chen and B. Cantrell, "Highly bandlimited radar signals," in *IEEE Radar Conference*, pp. 220–226, 1-3 April 2002.
- [17] J. de Graaf, H. H. Faust, J. Alatishe, and S. Talapatra, "Generation of spectrally confined transmitted radar waveforms: experimental results," in *IEEE Conference on Radar*, 24-27 April 2006.

- [18] S. Blunt, K. Gerlach, and T. Higgins, “Aspects of radar range super-resolution,” in *IEEE Radar Conference*, pp. 683–687, 17-20 April 2007.
- [19] T. Felhauer, “Digital signal processing for optimum wideband channel estimation in the presence of noise,” *IEE Proceedings of Radar and Signal Processing*, vol. 140, pp. 179–186, June 1993.